Parabolic lines and caustics in weakly anisotropic solids

Václav Vavryčuk

Geophysical Institute, Academy of Sciences of the Czech Republic, Boční II/1401, 141 31 Praha 4, Czech Republic, E-mail: vv@ig.cas.cz

Summary

The behaviour of parabolic lines and caustics in anisotropic solids can be, in general, very complicated, but it considerably simplifies under weak anisotropy. Supposing sufficiently weak anisotropy, no parabolic lines appear on the *S*1 slowness sheet. Consequently, the *S*1 wave sheet displays no caustics and triplications. Parabolic lines and caustics can appear for the *S*2 wave, but only in the directions close to conical or wedge singularities. Each conical and wedge singularity in weakly anisotropic solids generates parabolic lines, caustics and anticaustics in its vicinity. The parabolic lines cannot touch or pass through a conical singularity, but they touch each wedge singularity. For decreasing strength of anisotropy, the size of caustics and anticaustics decreases. For infinitesimally weak anisotropy, the caustics and anticaustics contract into one joint point. No parabolic lines, caustics, anticaustics and triplications can appear in transversely isotropic solids, provided the strength of anisotropy is sufficiently weak.

1. Introduction

Caustics often cause difficulties in modeling of wave fields. They produce infinite ray amplitudes, phase shifting of the ray-theoretical Green function (Bakker 1998) and triplications of the wave front. The caustics usually appear in wave fields propagating in inhomogeneous media like gradient media or media with curved interfaces. But in principle, they can appear even in homogeneous media, if the medium displays anisotropy (Musgrave 1970; Helbig 1994). The existence of caustics and triplications in homogeneous anisotropic media is conditioned by existence of parabolic lines on the slowness surface. These lines are formed by points of the zero Gaussian curvature and separate convex, concave and hyperbolic areas on the slowness surface (Every & Kim 1994). The parabolic lines on the slowness surface can uniquely be mapped onto the caustics on the wave surface; hence the shape of the slowness surface fully determines the shape of the wave surface including all caustics and triplications. The behaviour of parabolic lines and caustics in strongly anisotropic media can be very complicated (see Figs 1 and 2). Generally, the stronger anisotropy is, the more complicated pattern of parabolic lines and caustics can be expected. Peculiarities in the pattern of parabolic lines and caustics also arise in the vicinity of acoustic axes (Musgrave 1985; Boulanger & Hayes 1998; Shuvalov 1998) sometimes called singularity directions (Crampin & Yedlin 1981). The slowness sheets of two waves touch or intersect in these

directions and can display anomalous shape in their vicinity (Grechka & Obolentseva 1993; Vavryčuk 2001). This concerns particularly the conical singularity, which is likely one of the most complicated singularities in anisotropy (Burridge 1967; Shuvalov & Every 1994; Rümpker & Thomson 1994).

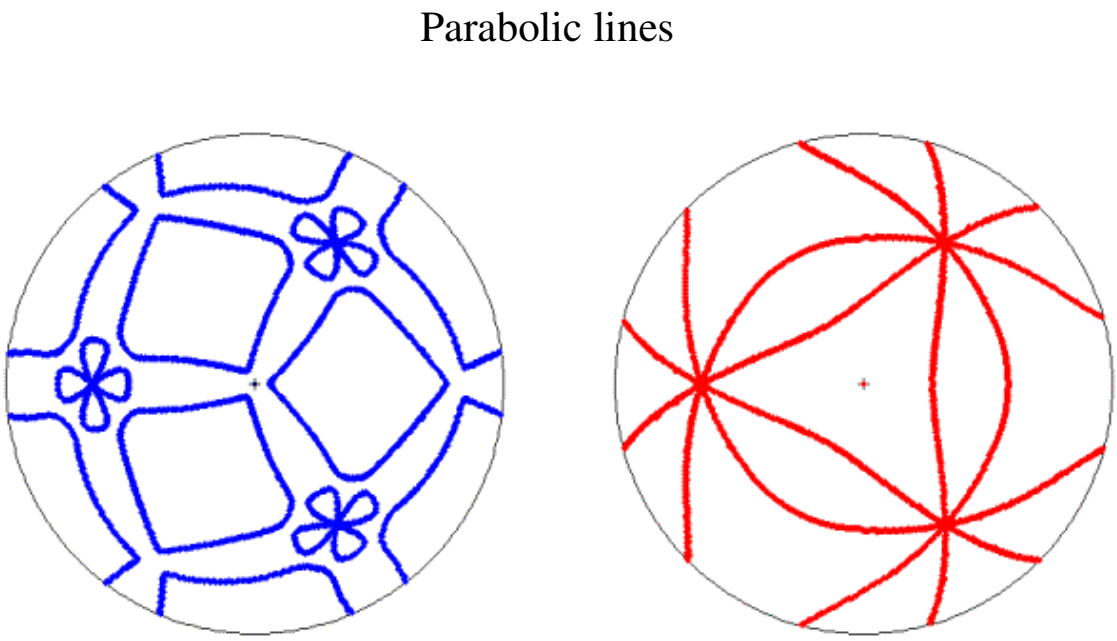

Figure 1. Parabolic lines on the slowness sheets for the *S*1 (right) and *S*2 (left) waves in strong cubic anisotropy. Parameters of anisotropy are: $a_{11} = 6.25$, $a_{44} = 2.08$, $\gamma = a_{12} - a_{11} + 2a_{44} = 2.00$. The medium is rotated the conical singularity to coincide with the vertical axis. The equal-area projection is used (see Aki & Richards 1980, Fig. 4.17). The cross marks the vertical axis. The circles correspond to deviations of 90° of slowness directions from the vertical axis.

In this paper, we shall study behaviour of parabolic lines and caustics in weakly anisotropic media. The condition of weak anisotropy is well satisfied for most rocks and geological structures in the Earth (Thomsen 1986) and considerably simplifies the problem. Obviously, if anisotropy is weak, the shape of the slowness surface should be more regular and behaviour of parabolic lines and caustic should simplify. If anisotropy vanishes and medium becomes isotropic, the parabolic lines and caustics disappear. We shall study the shape of the slowness surface by means of the metric tensor (Červený 2002). This tensor can be specified under weak anisotropy using perturbation theory (Jech & Pšenčík 1989; Pšenčík 1996; Farra 2001). Perturbation theory will also be used for studying the metric tensor near singularities (Shuvalov 1998). In the paper, we shall address particularly the following questions: Do parabolic lines and caustics disappear in weakly anisotropic solids? How the parabolic lines and caustics behave in dependence on strength of anisotropy? Are parabolic

lines and caustics connected with existence of singularities? Can parabolic lines or caustics touch or pass through a singularity in weakly anisotropic solids? Can caustics touch anticaustics?

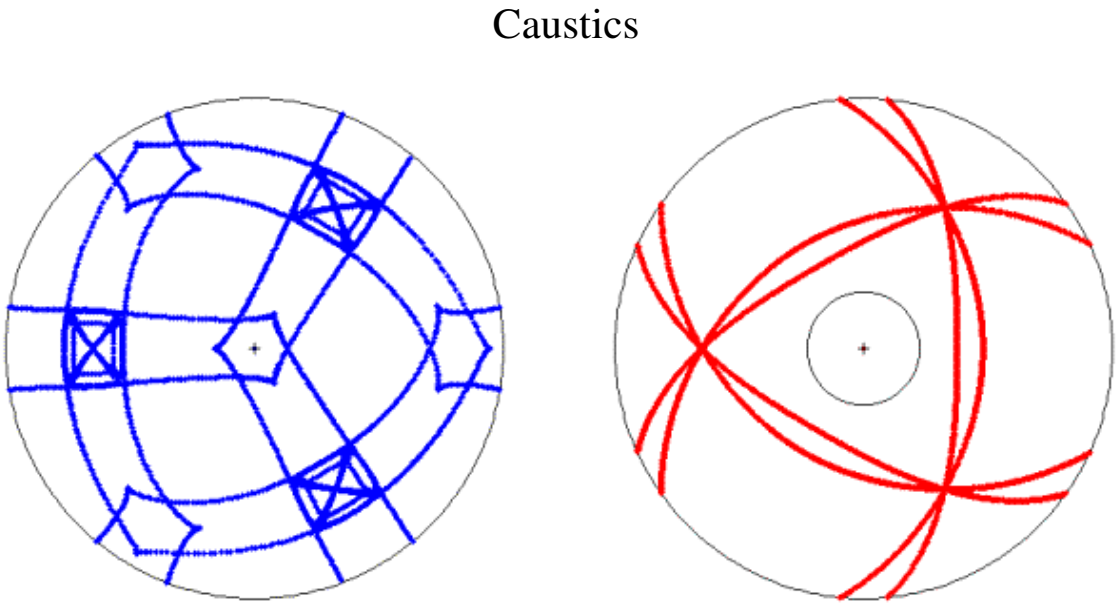

Figure 2. Caustics on the wave sheets for the *S*1 (right) and *S*2 (left) waves in strong cubic anisotropy. For parameters of the medium, see the caption of Fig. 1. The inner circle denotes the anticaustic. The cross marks the vertical axis. The outer circles correspond to deviations of 90° of ray directions from the vertical axis.

2. Slowness and wave surfaces

The elastic properties of homogeneous anisotropic media are described by elasticity tensor c_{ijkl} or by density-normalized elasticity tensor $a_{ijkl} = c_{ijkl} / \rho$, where ρ is the density of the medium. These tensors control the shapes of the slowness surface *S* and of the wave surface *W*.

2.1. Slowness surface

The slowness surface *S* is determined by the equation (Červený 2001, Eqs 2.2.35-37)

$$\det\left(\Gamma_{jk} - G\delta_{jk}\right) = 0\,, \tag{1}$$

where Γ_{jk} is the Christoffel tensor, and *G* is its eigenvalue

$$G = \Gamma_{jk} g_j g_k \ . \tag{2}$$

Vector **g** is the unit polarization vector calculated as the eigenvector of Γ_{jk}. The Christoffel tensor Γ_{jk} can be defined either by slowness direction **n**

$$\Gamma_{jk}(\mathbf{n}) = a_{ijkl} n_i n_l \ , \tag{3}$$

or by slowness vector $\mathbf{p} = \mathbf{n}/c$, where c is the phase velocity of the wave,

$$\Gamma_{jk}(\mathbf{p}) = a_{ijkl} p_i p_l \ . \tag{4}$$

The eigenvalues $G(\mathbf{n})$ and $G(\mathbf{p})$ read

$$G(\mathbf{n}) = a_{ijkl} n_i n_l g_j g_k = c^2 \ , \tag{5}$$

$$G(\mathbf{p}) = a_{ijkl} p_i p_l g_j g_k = 1 \ . \tag{6}$$

In the next, we shall implicitly assume G and Γ_{jk} dependent on direction **n**, until the dependence on slowness vector **p** is explicitly written.

Since the Christoffel tensor has three eigenvalues, the slowness surface consists of three sheets corresponding to three different waves (*P*, *S*1 and *S*2 waves). These sheets can be separated, but they can also touch or intersect each other. The degree of the slowness surface is 6, thus any straight line intersects *S* at most in 6 points. This implies that any detached inner sheet of *S* (corresponding to the *P* wave) must be wholly convex, because if it were not, a line could intersect the inner sheet in 4 or more points and yet at least 4 further intersections with the remaining sheets (see Musgrave 1970, p. 92). In contrast to the inner sheet, the other sheets can be also locally concave or hyperbolic.

2.2. Wave surface

The wave surface *W* is determined by the equation (Červený 2001, Eq. 2.2.65)

$$v_i = \frac{1}{2} \frac{\partial G(\mathbf{p})}{\partial p_i} = a_{ijkl} p_l g_j g_k \ , \tag{7}$$

where $\mathbf{v} = \mathbf{N}v$ means the group-velocity vector, v is the group velocity, and **N** is the ray direction. In contrary to the slowness surface, the geometry of the wave surface is much more complicated. The degree of *W* may be significantly higher than that of *S* (but must be less than 150; see Musgrave 1970, p. 92). Moreover, if the slowness sheet of the studied wave contains hyperbolic or concave areas, function $\mathbf{v} = \mathbf{v}(\mathbf{p})$ can be multivalued. This means that many group-velocity vectors can correspond to one specified slowness vector. This effect is known as the "triplication" of the wave surface.

2.3. Parabolic lines and caustics

It follows from (7) that the geometry of the wave surface is fully controlled by the geometry of the slowness surface. If the slowness sheet of a particular wave is wholly convex than the corresponding wave surface is also wholly convex and displays no triplications. As mentioned, the triplications arise when some areas on the slowness sheets are concave or hyperbolic (see Fig. 3). The shape of the slowness surface is conveniently classified by the sign of the Gaussian curvature: the elliptic (convex or concave) points on the surface have a positive Gaussian curvature, the hyperbolic points have a negative Gaussian curvature. The zero Gaussian curvature defines the parabolic points. The parabolic points form parabolic lines that are boundaries between the convex, concave and hyperbolic areas. Since the Gaussian curvatures of the slowness and wave surfaces are related by the following equation (Grechka & Obolentseva 1993, Eq. 17; Vavryčuk & Yomogida 1996, Eq. B.6)

$$K^S K^W = (\mathbf{n}\cdot\mathbf{N})^4, \tag{8}$$

it is obvious that the elliptic/hyperbolic points on *S* project into the elliptic/hyperbolic points on *W* (see Tab. 1). The parabolic lines with the zero Gaussian curvature on *S* project into the cuspidal line edges with the infinite Gaussian curvature on *W*, called "caustics" (see Fig. 3). Finally, points with the infinite Gaussian curvature on *S*, which are known as the conical singularities or conical points (Shuvalov 1998), are projected into the lines with the zero Gaussian curvature on *W*, called "anticaustics" (Shuvalov & Every 1997).

Figure 4 shows geometry of slowness and wave surfaces around a conical singularity in Payton's transverse isotropy (Payton 1992). This anisotropy forms a conical singularity along the symmetry axis. The conical singularity on the slowness surface (left-hand plots) projects onto a circular anticaustic, which separates wave sheets of the *P* and *SV* waves (right-hand plots). On the other hand, the circular parabolic lines separating convex and hyperbolic areas on the slowness surface (points 1, 3, 4 and 6 in the left-hand plots) contract into the conical caustic along the symmetry axis in the wave surface (right-hand plots). Notice that the wave sheet for the *P* wave is not defined for all ray directions.

Table 1. Shapes of the slowness and wave surfaces.

Slowness surface	Curvature K^S	Curvature K^W	Wave surface
Elliptic point	$K^S > 0$	$K^W > 0$	Elliptic point
Hyperbolic point	$K^S < 0$	$K^W < 0$	Hyperbolic point
Parabolic point	$K^S = 0$	$K^W = \pm\infty$	Caustic
Conical point	$K^S = \pm\infty$	$K^W = 0$	Anticaustic

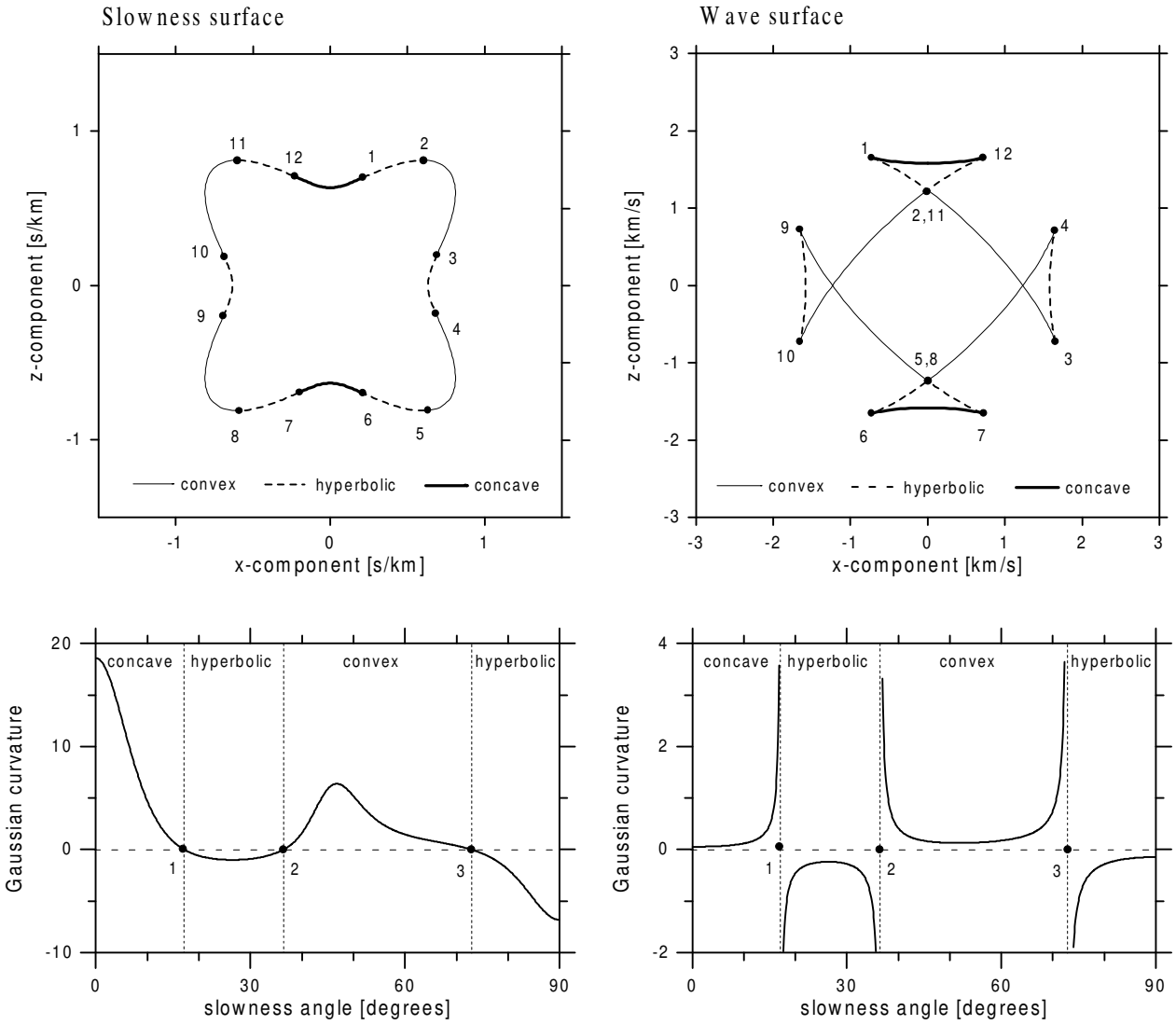

Figure 3. Parabolic points on the slowness sheet (upper left), triplications and caustics on the wave sheet (upper right) and Gaussian curvatures of the slowness (lower left) and wave (lower right) sheets for the *SV* wave in transverse isotropy. Parameters of the medium are: $a_{11} = a_{22} = a_{33} = 6.25$, $a_{44} = a_{55} = a_{66} = 2.50$, $a_{12} = 1.25$ and $a_{13} = a_{23} = 4.50$. The slowness angle is the angle between the slowness direction and the symmetry axis that coincides with the vertical axis. Parabolic points (left-hand plots) and caustics (right-hand plots) are marked by dots.

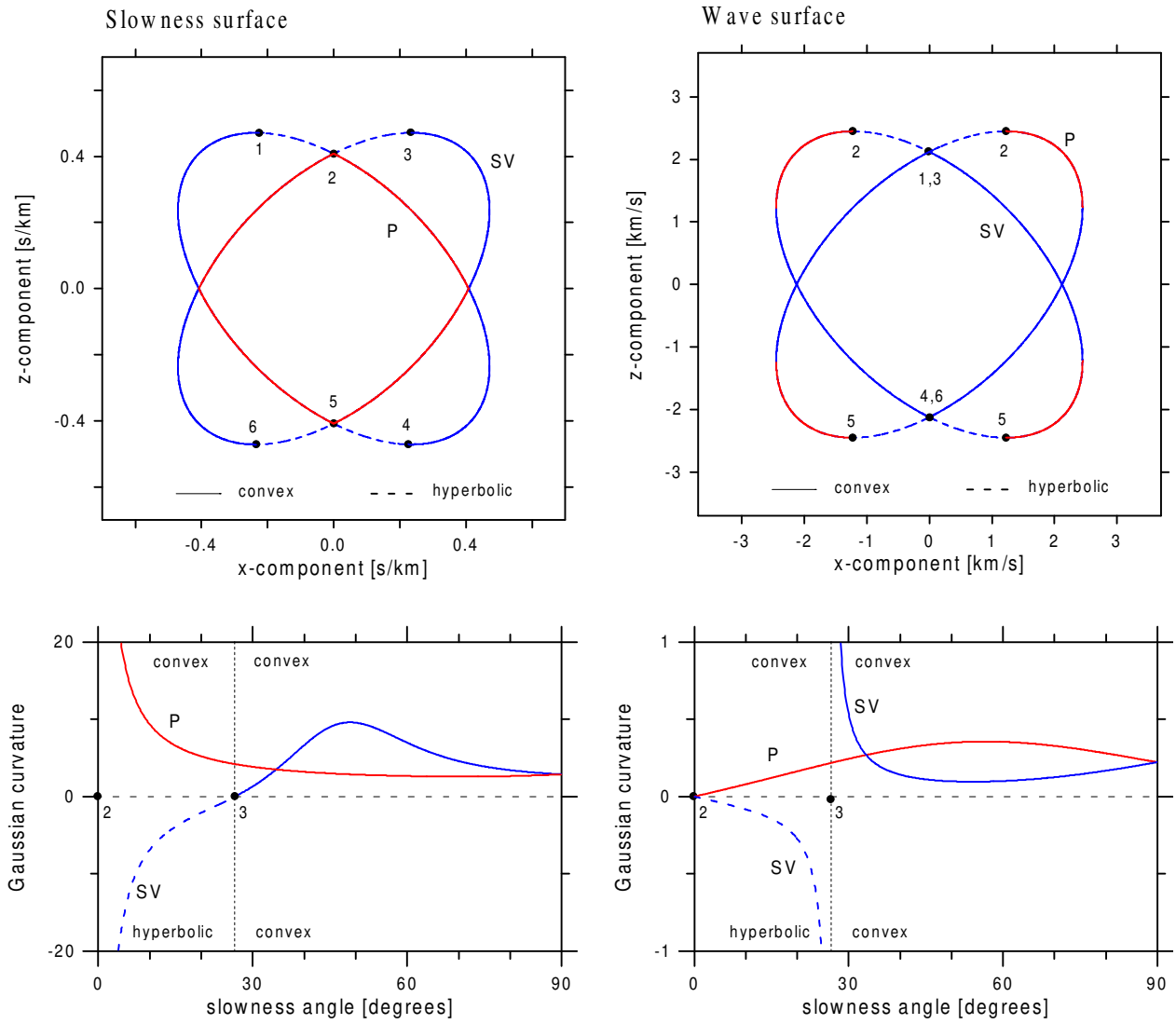

Figure 4. Slowness sheets (upper left), wave sheets (upper right) and Gaussian curvatures of the slowness (lower left) and wave (lower right) sheets are shown for the *P* and *SV* waves in Payton's transverse isotropy displaying a conical singularity along the symmetry axis. Parameters of the medium are: $a_{11} = a_{22} = a_{33} = a_{44} = a_{55} = 6.00$, $a_{66} = 3.00$ and $a_{12} = a_{13} = a_{23} = 0$. The slowness angle is the angle between the slowness direction and the symmetry axis that coincides with the vertical axis. Left-hand plots: points (1) and (3) are parabolic points, point (2) is the conical singularity. Right-hand plots: points (1) and (3) coincide with the conical caustic, point (2) marks the anticaustic.

3. Metric tensor in general anisotropy

We define the metric tensor in anisotropic homogeneous media as follows

$$H_{il}(\mathbf{p}) = \frac{\partial^2 H(\mathbf{p})}{\partial p_i \partial p_l} = \frac{1}{2}\frac{\partial^2 G(\mathbf{p})}{\partial p_i \partial p_l}, \tag{9}$$

where $H(\mathbf{p}) = \frac{1}{2}G(\mathbf{p})$ means the modified Hamiltonian (see Červený 2002) and $G(\mathbf{p})$ is the eigenvalue of the Christoffel tensor $\Gamma_{jk}(\mathbf{p})$. For inhomogenous media, metric tensor $H_{kl}(\mathbf{p})$, Hamiltonian $H(\mathbf{p})$ and eigenvalue $G(\mathbf{p})$ are also functions of the position vector **x**. The determinant of the metric tensor is simply connected to the shape of the slowness surface: $\det(H_{kl}) > 0$ for elliptic points, $\det(H_{kl}) < 0$ for hyperbolic points, and $\det(H_{kl}) = 0$ for parabolic points of the slowness surface.

From eqs (7) and (9) we can write the metric tensor in general anisotropic media in the following form:

$$H_{il}^{(s)}(\mathbf{p}) = \frac{\partial v_i^{(s)}}{\partial p_l} = a_{ijkl} g_j^{(s)} g_k^{(s)} + a_{ijkm} p_m \frac{\partial}{\partial p_l}\left(g_j^{(s)} g_k^{(s)}\right), \tag{10}$$

where superscript s (s = 1,2,3) denotes the type of the wave (*P*, *S*1, *S*2). Expressing the derivative of the *P*-wave polarization vector $\mathbf{g}^{(1)}$ as (see Červený 2001, Eqs 4.14.8-10)

$$\frac{\partial g_i^{(1)}}{\partial p_l} = \frac{\partial \Gamma_{jk}(\mathbf{p})}{\partial p_l} g_j^{(1)} \left[\frac{g_k^{(2)} g_i^{(2)}}{G^{(1)}(\mathbf{p}) - G^{(2)}(\mathbf{p})} + \frac{g_k^{(3)} g_i^{(3)}}{G^{(1)}(\mathbf{p}) - G^{(3)}(\mathbf{p})}\right], \tag{11}$$

and taking into account that

$$\frac{\partial \Gamma_{jk}(\mathbf{p})}{\partial p_l} = \left(a_{ijkl} + a_{ikjl}\right) p_i \ , \tag{12}$$

$$\left(a_{ijkl} + a_{ikjl}\right) p_i g_j^{(r)} g_k^{(s)} = a_{ijkl} p_i \left(g_j^{(r)} g_k^{(s)} + g_j^{(s)} g_k^{(r)}\right), \ r, s = 1,2,3, \tag{13}$$

we finally obtain for the metric tensor of the *P* wave

$$H_{il}^{(1)}(\mathbf{p}) = a_{ijkl} g_j^{(1)} g_k^{(1)} + \frac{v_i^{(12)}(\mathbf{p}) v_l^{(12)}(\mathbf{p})}{G^{(1)}(\mathbf{p}) - G^{(2)}(\mathbf{p})} + \frac{v_i^{(13)}(\mathbf{p}) v_l^{(13)}(\mathbf{p})}{G^{(1)}(\mathbf{p}) - G^{(3)}(\mathbf{p})}, \tag{14}$$

where $\mathbf{v}^{(rs)}(\mathbf{p})$, r, s = 1,2,3, is defined as

$$v_i^{(rs)}(\mathbf{p}) = a_{ijkl}\, p_l \left(g_j^{(r)} g_k^{(s)} + g_j^{(s)} g_k^{(r)} \right). \tag{15}$$

Formulae for the metric tensors of the *S*1 and *S*2 waves are quite analogous to (14). It can be shown that formula (14) is invariant to substituting $G(\mathbf{p})$ and $\mathbf{v}^{(rs)}(\mathbf{p})$ by $G(\mathbf{n})$ and $\mathbf{v}^{(rs)}(\mathbf{n})$. Hence, we express the final formulae as follows:

$$H_{il}^{(1)} = a_{ijkl} g_j^{(1)} g_k^{(1)} + \frac{v_i^{(12)} v_l^{(12)}}{G^{(1)} - G^{(2)}} + \frac{v_i^{(13)} v_l^{(13)}}{G^{(1)} - G^{(3)}} \ , \tag{16}$$

$$H_{il}^{(2)} = a_{ijkl} g_j^{(2)} g_k^{(2)} + \frac{v_i^{(12)} v_l^{(12)}}{G^{(2)} - G^{(1)}} + \frac{v_i^{(23)} v_l^{(23)}}{G^{(2)} - G^{(3)}}, \tag{17}$$

$$H_{il}^{(3)} = a_{ijkl} g_j^{(3)} g_k^{(3)} + \frac{v_i^{(13)} v_l^{(13)}}{G^{(3)} - G^{(1)}} + \frac{v_i^{(23)} v_l^{(23)}}{G^{(3)} - G^{(2)}} \ , \tag{18}$$

where

$$v_i^{(rs)} = a_{ijkl} n_l \left(g_j^{(r)} g_k^{(s)} + g_j^{(s)} g_k^{(r)} \right), \tag{19}$$

$$G^{(s)} = a_{ijkl} n_i n_l g_j^{(s)} g_k^{(s)} \ , \tag{20}$$

and $\mathbf{g}^{(s)}$ is the polarization vector of the *s*-th wave.

We can readily prove from (16) that the *P*-wave slowness sheet must be wholly convex. Taking into account that: (1) tensor $a_{ijkl} g_j^{(1)} g_k^{(1)}$ is positively definite, (2) dyadics $v_i^{(rs)} v_l^{(rs)}$ has two zero eigenvalues and one non-zero eigenvalue which is always positive, and (3) eigenvalue $G^{(1)}$ is greater than or equal to $G^{(2)}$ and $G^{(3)}$, $G^{(1)} \geq G^{(2)} \geq G^{(3)}$; we obtain that $\det\left(H_{il}^{(1)}\right)$ must be positive for any slowness direction **n**. Hence, we can generalize the result obtained by Musgrave (1970, p. 92) about convexity of the *P*-wave slowness sheet: the *P*-wave slowness sheet must be convex even in cases when it touches slowness sheets of one or two other waves.

However, no conclusion similar to that for the *P* wave can be drawn for the *S*1 or *S*2 waves. As regards the *S*1 wave, the second term in (17) has a negative eigenvalue and can cause that $\det\left(H_{il}^{(2)}\right)$ is zero or negative for some slowness directions **n**. As regards the *S*2 wave, both the second and third terms in (18) have negative eigenvalues and can cause that $\det\left(H_{il}^{(3)}\right)$ is zero or negative for some slowness directions **n**. Therefore, parabolic lines can appear on the *S*1- as well as *S*2-wave slowness sheets. Furthermore, we can expect that the concave or hyperbolic areas on the slowness sheets will be larger for the *S*2 wave than for the *S*1 wave and that the parabolic lines should be, in general, more complicated for the *S*2 wave than for the *S*1 wave. Subsequently, geometry of the wave sheet for the *S*2 wave should also be more complicated than that for the *S*1 wave.

In contrary to anisotropy, metric tensor H_{il} is much more simple in isotropy. Taking into account that the group velocity is expressed as

$$v_i = c^2 p_i \ , \tag{21}$$

we obtain

$$H_{il} = \frac{\partial v_i}{\partial p_l} = c^2 \delta_{il} \ , \tag{22}$$

where c is the phase velocity of the wave, and δ_{il} is the Kronecker delta. Hence, $\det(H_{il})$ is always positive. Obviously, the slowness sheets are wholly convex and no parabolic lines can appear for *P* as well as *S* waves.

4. Parabolic lines in weak anisotropy

Here, we shall study the determinant of metric tensor H_{il} for the *S*1 and *S*2 waves in weakly anisotropic media. Since $\det(H_{il})$ is very simple under isotropy (22), we expect that it will not be very complicated even under weak anisotropy. To prove this we shall apply the first-order perturbation theory. Since the Christoffel tensor Γ_{jk} is degenerate in isotropy, we have to apply the perturbation theory for a degenerate Christoffel eigenvalue problem (see Appendix A) and specify eigenvalues and eigenvectors of Γ_{jk} under weak anisotropy (see Appendix B). Then we can linearize all necessary quantities in (17) and (18) to get the metric tensors for the *S*1 and *S*2 waves.

Linearizing the *S*1-wave metric tensor $H_{il}^{(2)}$ given in (17) for weakly anisotropic media, we obtain (see Appendix D)

$$H_{il}^{(2)} = H_{il}^{0(2)} + \Delta H_{il}^{(2)}, \tag{23}$$

where $H_{il}^{0(2)}$ denotes the leading term of the metric tensor, and $\Delta H_{il}^{(2)}$ denotes its perturbation

$$H_{il}^{0(2)} = \beta^2 \delta_{il} \ , \tag{24}$$

$$\begin{aligned} \Delta H_{il}^{(2)} = {} & \Delta a_{ijkl} g_j^{0(2)} g_k^{0(2)} + \left(\alpha^2 - \beta^2\right)\left(\Delta g_i^{(2)} g_l^{0(2)} + g_i^{0(2)} \Delta g_l^{(2)}\right) - g_i^{0(2)} \Delta v_l^{(12)} - g_l^{0(2)} \Delta v_i^{(12)} \\ & - g_i^{0(2)} g_l^{0(2)} \left(\Delta G^{(2)} - \Delta G^{(1)}\right) + \frac{\Delta v_i^{(23)} \Delta v_l^{(23)}}{\Delta G} \ . \end{aligned} \tag{25}$$

The result for $H_{il}^{0(2)}$ was expected from (22). Vectors $\mathbf{g}^{0(s)}$, s = 1,2,3 are polarization vectors in an isotropic reference medium: vector $\mathbf{g}^{0(1)}$ is the *P*-wave polarization vector coinciding

with vector **n**, and vectors $\mathbf{g}^{0(2)}$ and $\mathbf{g}^{0(3)}$ form a special frame of orthonormal vectors perpendicular to $\mathbf{g}^{0(1)}$ satisfying the following continuity relations (see Appendix B):

$$\mathbf{g}^{(2)}\left(a_{ijkl}, n_i\right) \to \mathbf{g}^{0(2)}\left(a^0_{ijkl}, n_i\right) \text{ and } \mathbf{g}^{(3)}\left(a_{ijkl}, n_i\right) \to \mathbf{g}^{0(3)}\left(a^0_{ijkl}, n_i\right) \tag{26}$$

for vanishing anisotropy, $\Delta a_{ijkl} \to 0$.

Formulae for linearized *S*2-wave metric tensor $H^{0(3)}_{il}$ are quite analogous to (23)-(25). Finally, we arrive at the expression for $\det\left(H^{(J)}_{il}\right)$, *J* = 2,3:

$$\det\left(H^{(J)}_{il}\right) = \begin{vmatrix} \beta^2 + \Delta H^{(J)}_{11} & \Delta H^{(J)}_{12} & \Delta H^{(J)}_{13} \\ \Delta H^{(J)}_{12} & \beta^2 + \Delta H^{(J)}_{22} & \Delta H^{(J)}_{23} \\ \Delta H^{(J)}_{13} & \Delta H^{(J)}_{23} & \beta^2 + \Delta H^{(J)}_{33} \end{vmatrix} \sim \beta^6 \left(1 + \frac{\Delta H^{(J)}_{ii}}{\beta^2}\right), \tag{27}$$

$$\Delta H^{(2)}_{ii} = \Delta a_{ijki} g^{0(2)}_j g^{0(2)}_k - 2 g^{0(2)}_i \Delta v^{(12)}_i - \Delta G^{(2)} + \Delta G^{(1)} + \frac{\Delta v^{(23)}_i \Delta v^{(23)}_i}{\Delta G}, \tag{28}$$

$$\Delta H^{(3)}_{ii} = \Delta a_{ijki} g^{0(3)}_j g^{0(3)}_k - 2 g^{0(3)}_i \Delta v^{(13)}_i - \Delta G^{(3)} + \Delta G^{(1)} - \frac{\Delta v^{(23)}_i \Delta v^{(23)}_i}{\Delta G}, \tag{29}$$

where we omitted all terms with second- or higher-order perturbations and used in (24) and (25) the following identities:

$$g^{0(2)}_i \Delta g^{(2)}_i = 0, \quad g^{0(3)}_i \Delta g^{(3)}_i = 0.$$

Perturbation $\Delta \mathbf{v}^{(rs)}$ reads

$$\Delta v^{(rs)}_i = \Delta a_{ijkl} n_i \left(g^{0(r)}_j g^{0(s)}_k + g^{0(s)}_j g^{0(r)}_k\right) + a^0_{ijkl} n_l \left(\Delta g^{(r)}_j g^{0(s)}_k + g^{0(r)}_j \Delta g^{(s)}_k + \Delta g^{(s)}_j g^{0(r)}_k + g^{0(s)}_j \Delta g^{(r)}_k\right) \tag{30}$$

and perturbations of eigenvalues $\Delta G^{(s)}$ and eigenvectors $\Delta \mathbf{g}^{(s)}$ are in Appendix B.

Let us assume that slowness direction **n** points outside the *S*-wave singular regions, hence the slowness sheets of the *S*1 and *S*2 waves are non-degenerate ($\Delta G \neq 0$) and they do not touch or intersect each other in the vicinity of **n**. Then all terms on the right-hand sides of (28) and (29) are small being linear functions of Δa_{ijkl} and we can write

$$\frac{\Delta H^{(J)}_{ii}}{\beta^2} << 1 \quad , J = 2,3. \tag{31}$$

This implies that $\det\left(H^{(J)}_{il}\right)$ expressed in (27) must be positive and that the slowness sheets of the *S*1 or *S*2 waves must be convex in the studied directions. In other words, no parabolic

lines can appear on the $S1$ or $S2$ slowness sheets in weakly anisotropic media in directions outside the S-wave singular regions. In singularities ($\Delta G = 0$) and their vicinities, the last term in (28) and (29) may be large or even infinite. Since the sign of this term is positive for the $S1$ wave, we conclude that $\det\left(H_{il}^{(2)}\right)$ must be positive even in singular regions. Consequently, no parabolic lines can appear on the $S1$-wave slowness surface in weakly anisotropic media in all directions including singularities. On the other hand, the sign of the last term in (29) is negative for the $S2$ wave and it may cause that $\det\left(H_{il}^{(3)}\right)$ is zero or negative in the vicinity of a singularity. Therefore, behaviour of $H_{il}^{(3)}$ needs a special analysis in this case.

5. Parabolic lines near singularities in weak anisotropy

Examination of the shape of the $S2$-wave slowness sheet in weakly anisotropic media near S-wave singularities needs a special treatment. In regular directions, small perturbations Δa_{ijkl} result in small perturbations of all basic quantities of the wave fields including shapes of the slowness and wave surfaces. In directions close to a singularity, the behavior of the polarization vectors is, however, anomalous and it can cause also anomalies in shapes of the slowness and wave surfaces. As regards metric tensor $H_{il}^{(3)}$ defined in (18), the anomalies are caused by the following term:

$$H_{il}^{(23)} = \frac{v_i^{(23)} v_l^{(23)}}{\Delta G}, \tag{32}$$

because its denominator $\Delta G = G^{(2)} - G^{(3)}$ is zero in the singularity. The anomalous behaviour of $H_{il}^{(23)}$ near singularities can be studied using perturbation theory but in a slightly modified way as compared to the previous section. So far, we perturbed elastic parameters a_{ijkl},

$$a_{ijkl} = a_{ijkl}^0 + \Delta a_{ijkl}\ , \tag{33}$$

to obtain quantities in weak anisotropy expressed by those in isotropy. Now, we have to perturb slowness direction $\mathbf{n}$

$$\mathbf{n} = \mathbf{n}^0 + \Delta\mathbf{n}\ , \tag{34}$$

to obtain quantities in the close vicinity of a singularity expressed by those in the singularity. Both approaches are very similar, because the Christoffel tensor Γ_{jk} is degenerate in isotropy as well as in a singularity. Therefore, perturbation theory for a degenerate Christoffel eigenvalue problem (see Appendix A) has to be applied in both cases. However, specification of general formulae for eigenvalues and eigenvectors of Γ_{jk} is different for (33) and (34). The

perturbation formulae obtained by using (34) are in Appendix C. Using these formulae we can perturb $H_{il}^{(23)}$ in (32) to inspect its properties in the vicinity of a singularity. Perturbing $H_{il}^{(23)}$ we obtain

$$H_{il}^{(23)} = H_{il}^{0(23)} + \Delta H_{il}^{(23)} \ , \tag{35}$$

where $H_{il}^{0(23)}$ denotes the value of $H_{il}^{(23)}$ in the singularity, and $\Delta H_{il}^{(23)}$ is its perturbation. Inserting (32) into (35) we can write

$$H_{il}^{0(23)} = \frac{v_i^{0(23)} v_l^{0(23)}}{\Delta G} \ , \tag{36}$$

$$\Delta H_{il}^{(23)} = \frac{v_i^{0(23)} \Delta v_l^{(23)} + \Delta v_i^{(23)} v_l^{0(23)} + \Delta v_i^{(23)} \Delta v_l^{(23)}}{\Delta G} \tag{37}$$

where

$$\begin{aligned} v_i^{0(23)} &= a_{ijkl} n_l^0 \left(g_j^{0(2)} g_k^{0(3)} + g_j^{0(3)} g_k^{0(2)} \right) , \\ \Delta v_i^{(23)} &= a_{ijkl} \Delta n_l \left(g_j^{0(2)} g_k^{0(3)} + g_j^{0(3)} g_k^{0(2)} \right) + a_{ijkl} n_l^0 \left(\Delta g_j^{(2)} g_k^{0(3)} + g_j^{0(2)} \Delta g_k^{(3)} + \Delta g_j^{(3)} g_k^{0(2)} + g_j^{0(3)} \Delta g_k^{(2)} \right) \end{aligned} \tag{38}$$

Vectors $\mathbf{g}^{0(2)}$ and $\mathbf{g}^{0(3)}$ form a special frame of orthonormal vectors perpendicular to $\mathbf{g}^{0(1)}$ satisfying the following continuity relations:

$$\mathbf{g}^{(2)}\left(a_{ijkl}, n_i\right) \to \mathbf{g}^{0(2)}\left(a_{ijkl}, n_l^0\right) \text{ and } \mathbf{g}^{(3)}\left(a_{ijkl}, n_i\right) \to \mathbf{g}^{0(3)}\left(a_{ijkl}, n_l^0\right) \tag{39}$$

for **n** approaching singularity direction $\mathbf{n}^0$. Note that $\mathbf{v}^{0(23)}$ and $\Delta\mathbf{v}^{(23)}$ defined in (38) are slightly different quantities than those used in Sec. 4.

In the next, we shall evaluate $H_{il}^{0(23)}$ and $\Delta H_{il}^{(23)}$ for four kinds of the *S*-wave singularity: kiss, conical, wedge and intersection singularities.

5.1. Kiss singularity

The kiss singularity is defined as the direction in which slowness sheets of two waves touch tangentially at an isolated point. The wave sheets are also tangential at the kiss singularity and the group velocities coincide for both waves. The condition for this singularity can be expressed as follows (Shuvalov 1998):

$$\widehat{\mathbf{u}}^{0(23)} = 0 \ , \quad \widehat{\mathbf{v}}^{0(23)} = 0 \ , \tag{40}$$

where $\widehat{\mathbf{u}}^{0(23)}$ and $\mathbf{v}^{0(23)}$ read

$$\widehat{u}_i^{0(23)} = a_{ijkl} n_l^0 \left(\widehat{g}_j^{0(2)} \widehat{g}_k^{0(2)} - \widehat{g}_j^{0(3)} \widehat{g}_k^{0(3)} \right), \; \widehat{v}_i^{0(23)} = a_{ijkl} n_l^0 \left(\widehat{g}_j^{0(2)} \widehat{g}_k^{0(3)} + \widehat{g}_j^{0(3)} \widehat{g}_k^{0(2)} \right). \tag{41}$$

Vector $\mathbf{n}^0$ specifies the singularity direction, and vectors $\widehat{\mathbf{g}}^{0(2)}$ and $\widehat{\mathbf{g}}^{0(3)}$ form an arbitrary frame of orthogonal unit vectors perpendicular to the *P*-wave polarization vector in the singularity. The leading terms of ΔG and Φ read

$$\Delta G = \vartheta^2 \sqrt{\left(\mathbf{e}^{\mathrm{T}} \widehat{\mathbf{F}} \mathbf{e} \right)^2 + \left(\mathbf{e}^{\mathrm{T}} \widehat{\mathbf{G}} \mathbf{e} \right)^2}, \; \vartheta << 1, \tag{42}$$

$$\tan 2\Phi = \frac{\mathbf{e}^{\mathrm{T}} \widehat{\mathbf{G}} \mathbf{e}}{\mathbf{e}^{\mathrm{T}} \widehat{\mathbf{F}} \mathbf{e}}, \tag{43}$$

where $\mathbf{e}$ is the unit vector perpendicular to the singularity direction $\mathbf{n}^0$ and specifies the direction from which the singularity is approached. Angle ϑ is the angle between slowness direction $\mathbf{n}$ and singularity direction $\mathbf{n}^0$ (see Appendix C). Matrices $\widehat{\mathbf{F}}$ and $\widehat{\mathbf{G}}$ are defined in (C6) and (C7). Since $\widehat{\mathbf{v}}^{0(23)}$ in (40) is zero for any frame of vectors $\widehat{\mathbf{g}}^{0(2)}$ and $\widehat{\mathbf{g}}^{0(3)}$, it must be zero also for base vectors $\mathbf{g}^{0(2)}$ and $\mathbf{g}^{0(3)}$:

$$\mathbf{v}^{0(23)} = 0 \; . \tag{44}$$

Inserting (44) into (35)-(37) we obtain for the leading term of $H_{il}^{(23)}$

$$H_{il}^{(23)} = \frac{\Delta v_i^{(23)} \Delta v_l^{(23)}}{\Delta G} \; . \tag{45}$$

Since $\Delta \mathbf{v}^{(23)}$ defined in (38) is the first-order quantity, and ΔG in (42) is the second-order quantity in ϑ, the leading term of $H_{il}^{(23)}$ is independent of ϑ. Hence, $H_{il}^{(23)}$ is finite in the kiss singularity and its close vicinity, but it is not necessarily small. Therefore, this term can generate parabolic lines crossing the kiss singularity on the *S*2-wave slowness sheet. However, this concerns strong anisotropy only, because if we assume weak anisotropy and apply a similar approach as in Sec. 4, we can prove that $\Delta \mathbf{v}^{(23)}$ and ΔG are the first-order perturbations in Δa_{ijkl}. Consequently, $H_{il}^{(23)}$ must be small

$$H_{il}^{(23)} = \frac{\Delta v_i^{(23)} \Delta v_l^{(23)}}{\Delta G} << 1 \; . \tag{46}$$

Hence, no parabolic lines can appear on the *S*2-wave slowness sheet in the kiss singularity and its vicinity in weak anisotropy.

5.2. Conical singularity

The conical singularity is defined as the direction, in which two slowness sheets touch through the vertices of cone-shaped surfaces. The condition for this singularity can be expressed by means of the vector product of $\hat{\mathbf{u}}^{0(23)}$ and $\mathbf{v}^{0(23)}$ as follows (Shuvalov 1998):

$$\hat{\mathbf{u}}^{0(23)} \times \hat{\mathbf{v}}^{0(23)} \neq 0 \ , \tag{47}$$

where $\hat{\mathbf{u}}^{0(23)}$ and $\hat{\mathbf{v}}^{0(23)}$ are defined in (41). From (C4) and (C8) we obtain for leading terms of ΔG and Φ

$$\Delta G = 2\vartheta \sqrt{\left(\hat{\mathbf{u}}^{0(23)} \cdot \mathbf{e}\right)^2 + \left(\hat{\mathbf{v}}^{0(23)} \cdot \mathbf{e}\right)^2} \ , \tag{48}$$

$$\tan 2\Phi = \frac{\hat{\mathbf{v}}^{0(23)} \cdot \mathbf{e}}{\hat{\mathbf{u}}^{0(23)} \cdot \mathbf{e}} \ . \tag{49}$$

It follows from (47) that $\hat{\mathbf{v}}^{0(23)}$ is non-zero. This applies for any frame of vectors $\hat{\mathbf{g}}^{0(2)}$ and $\hat{\mathbf{g}}^{0(3)}$ including vectors $\mathbf{g}^{0(2)}$ and $\mathbf{g}^{0(3)}$, hence

$$\mathbf{v}^{0(23)} \neq 0 \ . \tag{50}$$

Since ΔG goes to zero in the singularity ($\vartheta \to 0$), we obtain from (36)

$$H_{il}^{0(23)} = \frac{v_i^{0(23)} v_l^{0(23)}}{\Delta G} \to \infty \ . \tag{51}$$

This implies that when approaching the singularity

$$\det\left(H_{il}^{(2)}\right) \to \infty \ , \tag{52}$$

$$\det\left(H_{il}^{(3)}\right) \to -\infty \ . \tag{53}$$

Since $\det\left(H_{il}^{(3)}\right)$ is minus infinity in the singularity, but it is positive outside the singular region, there must exist directions near the singularity for which $\det\left(H_{il}^{(3)}\right)$ is zero. It implies that the parabolic line forms a closed curve around the singularity. The shape and size of the line depends on symmetry and strength of anisotropy. For decreasing strength of anisotropy the parabolic line should contract being very close to the singularity. For infinitely weak anisotropy, the parabolic line and the singularity merge, and the singularity disappears.

5.3. Wedge singularity

The wedge singularity is defined as the direction, in which two slowness sheets touch through the vertices of wedge-shaped surfaces. The wedge singularity can arise from the conical singularity if one of semiaxes of the elliptical base of the cone goes to infinity. The condition for this singularity can be expressed as follows (Shuvalov 1998):

$$\hat{\mathbf{u}}^{0(23)} \times \hat{\mathbf{v}}^{0(23)} = 0 \ , \ \ \hat{\mathbf{u}}^{0(23)} \cdot \hat{\mathbf{u}}^{0(23)} + \hat{\mathbf{v}}^{0(23)} \cdot \hat{\mathbf{v}}^{0(23)} = const \neq 0 \, , \tag{54}$$

where $\hat{\mathbf{u}}^{0(23)}$ and $\hat{\mathbf{v}}^{0(23)}$ are parallel vectors perpendicular to direction $\mathbf{t}$ of the wedge

$$\hat{\mathbf{u}}^{0(23)} \| \hat{\mathbf{v}}^{0(23)} \perp \mathbf{t} \ . \tag{55}$$

The wedge singularity combines properties of the kiss and conical singularities. For direction $\mathbf{e}$ along $\mathbf{t}$,

$$\hat{\mathbf{u}}^{0(23)} \cdot \mathbf{e} = 0 \ , \tag{56}$$

the leading terms of ΔG and Φ are expressed by (42) and (43) derived for the kiss singularity. For direction $\mathbf{e}$ perpendicular to $\mathbf{t}$, however, the leading terms of ΔG and Φ are expressed by (48) and (49) derived for the conical singularity. It can be shown that $\mathbf{v}^{0(23)}$ in (36)-(37) is zero for $\mathbf{e} \| \mathbf{t}$, but non-zero for $\mathbf{e} \perp \mathbf{t}$. Therefore, assuming weak anisotropy we can write for $\mathbf{e} \perp \mathbf{t}$,

$$H_{il}^{(23)} \to 0 \, , \ \ \det\left(H_{il}^{(3)}\right) \to \beta^6 \ , \tag{57}$$

and for $\mathbf{e} \| \mathbf{t}$,

$$H_{il}^{0(23)} \to \infty \, , \ \det\left(H_{il}^{(3)}\right) \to -\infty \ . \tag{58}$$

Hence, the *S*2-wave slowness sheet is always convex for directions $\mathbf{e}$ close to wedge direction $\mathbf{t}$, but hyperbolic for direction $\mathbf{e}$ perpendicular to $\mathbf{t}$. This implies that the wedge singularity generates parabolic lines in weakly anisotropic solids. These lines must always touch the singularity.

5.4. Intersection singularity

The intersection singularity occurs, when the slowness sheets of the *S*1 and *S*2 waves intersect along a line. This singularity is, in fact, a line wedge singularity. The condition for this singularity can be expressed as follows (Shuvalov 1998, Eq. 2.61):

$$\hat{\mathbf{v}}^{0(23)} = \eta \, \hat{\mathbf{u}}^{0(23)} \ , \ \mathbf{e}^{\mathrm{T}} \hat{\mathbf{G}} \mathbf{e} = \eta \, \mathbf{e}^{\mathrm{T}} \hat{\mathbf{F}} \mathbf{e} \ , \tag{59}$$

where η is a constant, vectors $\hat{\mathbf{u}}^{0(23)}$ and $\hat{\mathbf{v}}^{0(23)}$ are defined in (41), and matrices $\hat{\mathbf{F}}$ and $\hat{\mathbf{G}}$ are defined in (C6) and (C7). The base vectors $\hat{\mathbf{g}}^{0(2)}$ and $\hat{\mathbf{g}}^{0(3)}$ in (59) must be chosen to provide

$$\left| \hat{\mathbf{u}}^{0(23)} \right| \neq 0 \ . \tag{60}$$

Using (C4) and (C8) we can write the leading terms of ΔG and Φ as follows:

$$\Delta G = 2\vartheta \left(\hat{\mathbf{u}}^{0(23)} \cdot \mathbf{e} \right) \sqrt{1+\eta^2} \ , \tag{61}$$

$$\tan 2\Phi = \eta \ . \tag{62}$$

The intersection singularity displays no singular behaviour of polarization vectors in its vicinity (Shuvalov 1998), hence angle Φ is constant independently of direction $\mathbf{e}$ from which the singularity is approached. If we use base vectors $\mathbf{g}^{0(2)}$ and $\mathbf{g}^{0(3)}$ in (62), angle Φ is zero that implies η to be also zero. Hence from (59)

$$\mathbf{v}^{0(23)} = 0 \tag{63}$$

for any vector $\mathbf{e}$. Inserting (63) into (35)-(37) we obtain

$$H_{il}^{(23)} = \frac{\Delta v_i^{(23)} \Delta v_l^{(23)}}{\Delta G} \ . \tag{64}$$

Since $\Delta \mathbf{v}^{(23)}$ defined in (38) and ΔG defined in (61) are the first-order quantities in ϑ, we get

$$H_{il}^{(23)} << 1 \, . \tag{65}$$

This implies that $H_{il}^{(23)}$ produces no anomalies in the shape of the slowness sheet in the vicinity of the intersection singularity. Consequently, no parabolic lines can appear in the vicinity of this singularity in weakly anisotropic solids.

6. Examples

In this section, we shall demonstrate numerically results obtained in the previous section. We shall illustrate behaviour of parabolic lines and caustics on several examples of anisotropy displaying various symmetries and strengths. We shall concentrate on the vicinity of singularities, where the behaviour of parabolic lines and caustics is most complicated.

6.1. Kiss singularity

Figures 5 and 6 show behaviour of parabolic lines and caustics near a kiss singularity in cubic anisotropy. The kiss singularity is along the vertical axis. Anisotropy displays two different strengths: right-hand plots show strong anisotropy with anisotropy parameter γ being 1.38, and left-hand plots show very strong anisotropy with γ being 2.50. Figure 5 shows parabolic lines (upper plots) and caustics (lower plots) for the *S*2 wave, Fig. 6 shows the same for the *S*1 wave.

The first example of cubic anisotropy (left-hand plots) illustrates the case, when the *S*2-wave parabolic lines are around the singularity but do not touch the singularity. On the other hand, the *S*1-wave parabolic lines cross the singularity (see Fig. 6). This implies that the parabolic lines on the *S*1 and *S*2 slowness sheets behave independently and that the parabolic lines on the *S*1 slowness sheet only touch the singularity, but do not pass through the singularity. If the lines pass through the singularity, they should jump from one slowness sheet to the other, which is not the case.

The second example of anisotropy (right-hand plots) illustrates the case, when parabolic lines touch the singularity simultaneously on both slowness sheets. It also shows that parabolic lines as well as caustics are significantly more complicated for the *S*2 wave than for the *S*1 wave.

As mentioned, the second example displays lower anisotropy than the first one. When anisotropy further decreases, the hyperbolic area on the *S*1-wave slowness sheet also decreases. For $\gamma = 1.33$, the *S*1-wave parabolic lines disappear near the singularity. They even disappear on the whole *S*1 slowness sheet under this anisotropy. For $\gamma = 1.17$, the parabolic lines disappear also near the singularity on the *S*2-wave slowness sheet. Nevertheless, *S*2-wave parabolic lines and caustics still remain in the area near a conical singularity (see the next example).

6.2. Conical singularity

Figures 7 and 8 show behaviour of parabolic lines and caustics near a conical singularity in cubic anisotropy with four different anisotropy strengths. Anisotropy parameter γ is 0.75, 0.60, 040 and 020, respectively. Anisotropy is rotated the conical singularity to be along the vertical axis. The figures show the *S*2-wave parabolic lines only, because no parabolic lines appear in the *S*1-wave slowness sheet in these anisotropy models. Three pairs of parabolic lines appear on the *S*2 slowness sheet in the strongest anisotropy model studied (Fig. 7, left-hand plots). For decreasing anisotropy, the pairs of parabolic lines interconnect into one closed curve around the singularity (Fig. 7, right-hand plot). If anisotropy is further decreased (Fig. 8), the hyperbolic area inside the curve decreases and the curve concentrates in closer and closer vicinity of the singularity. However, it never disappears for non-zero anisotropy. The parabolic line can only disappear together with the singularity when anisotropy parameter γ is exactly zero, hence when medium becomes isotropic.

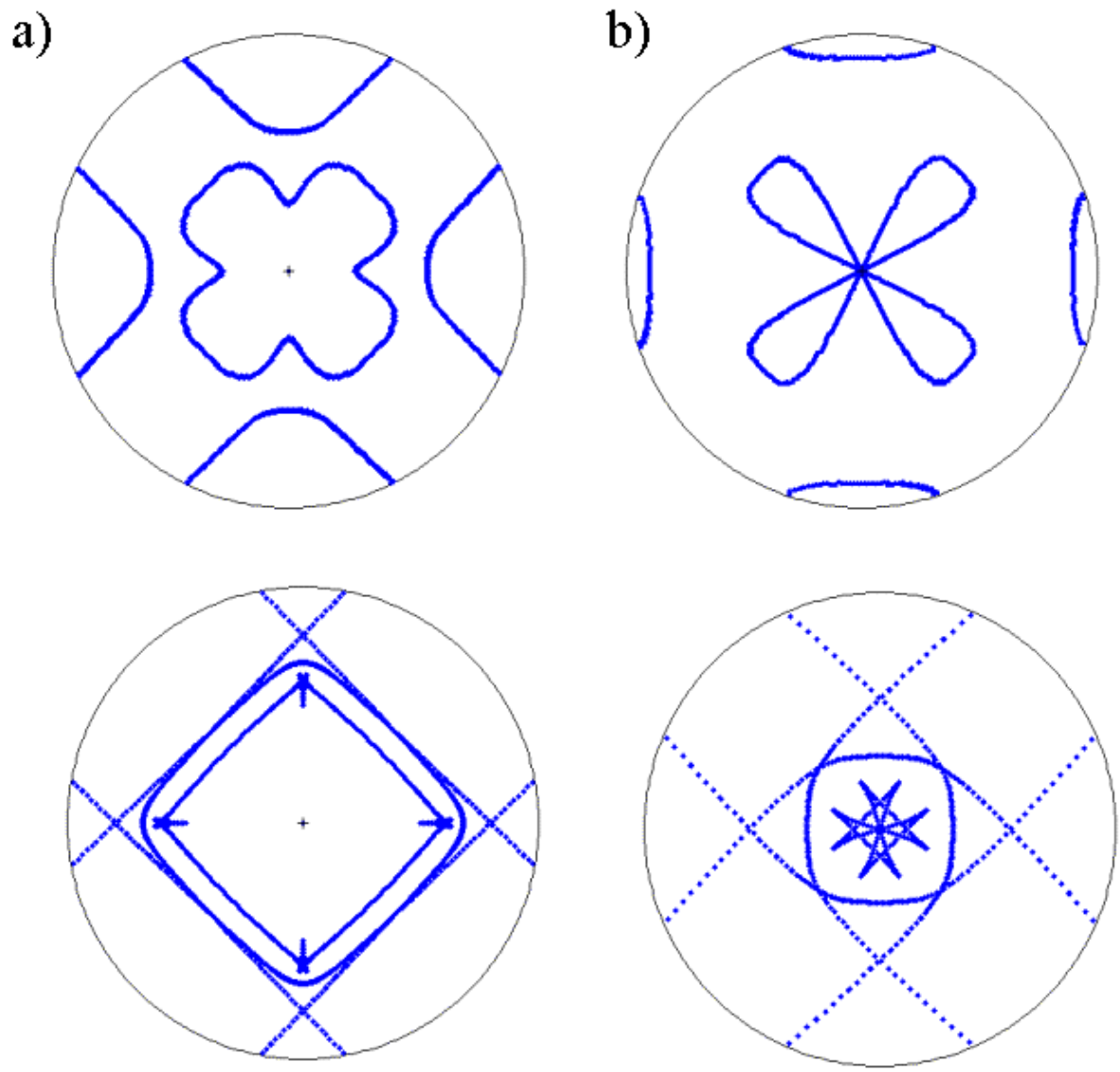

Figure 5. Parabolic lines (upper plots) and caustics (lower plots) for the *S*2 wave near the kiss singularity in cubic anisotropy. Parameters of anisotropy are: $a_{11} = a_{22} = a_{33} = 6.25$, $a_{44} = a_{55} = a_{66} = 2.08$, (a) $\gamma = 2.50$, (b) $\gamma = 1.38$, where γ is defined as $\gamma = a_{12} - a_{11} + 2a_{44}$. Parameter γ measures strength of anisotropy. The cross denotes the kiss singularity that coincides with the vertical axis. The circles correspond to the deviation (a) $\vartheta = 30°$, (b) $\vartheta = 13°$ of slowness directions (upper plots) or ray directions (lower plots) from the vertical axis.

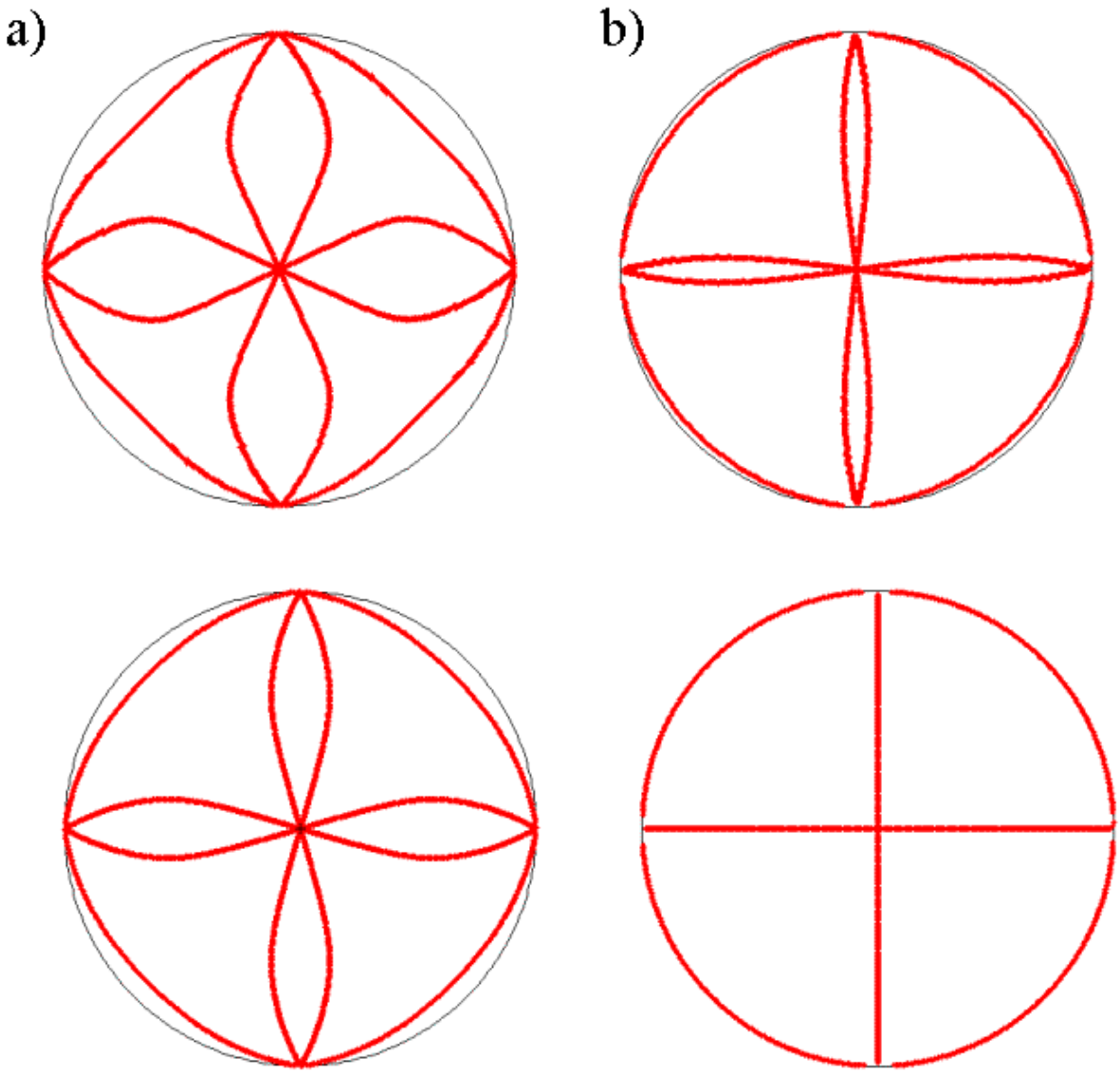

Figure 6. Parabolic lines (upper plots) and caustics (lower plots) for the *S*1 wave near the kiss singularity in cubic anisotropy. Parameters of anisotropy are: $a_{11} = 6.25$, $a_{44} = 2.08$, (a) $\gamma = 2.50$, (b) $\gamma = 1.38$. The kiss singularity coincides with the vertical axis. The circles correspond to the deviation $\vartheta = 90°$ of slowness directions (upper plots) or ray directions (lower plots) from the vertical axis.

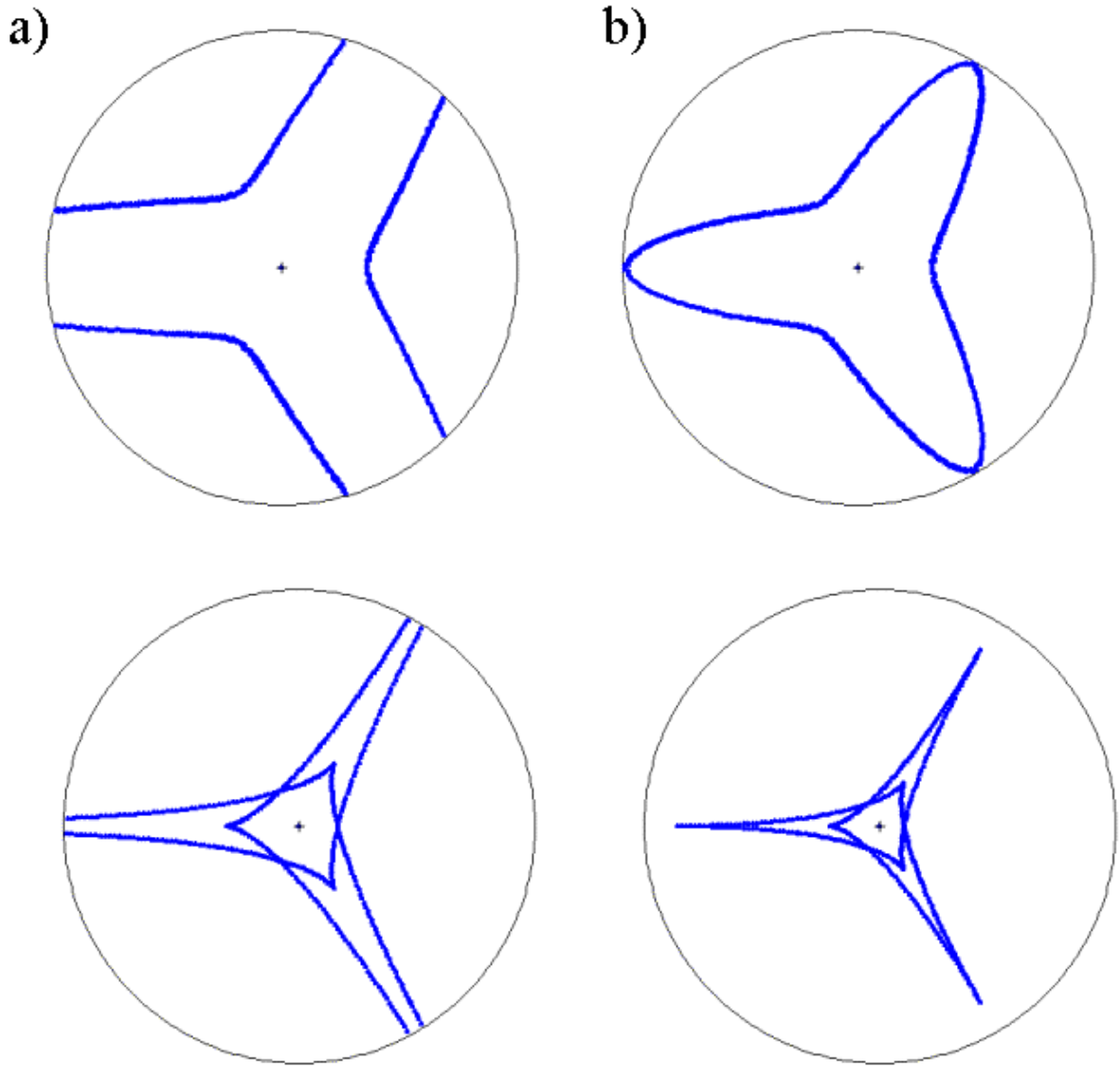

Figure 7. Parabolic lines (upper plots) and caustics (lower plots) for the *S*2 wave near the conical singularity in cubic anisotropy with varying strength. Parameters of anisotropy are: $a_{11} = 6.25$, $a_{44} = 2.08$, (a) $\gamma = 0.75$, (b) $\gamma = 0.60$. The crosses in upper plots denote the conical singularity that coincides with the vertical axis. The circles correspond to deviation $\vartheta = 8°$ of slowness directions (upper plots) or ray directions (lower plots) from the vertical axis.

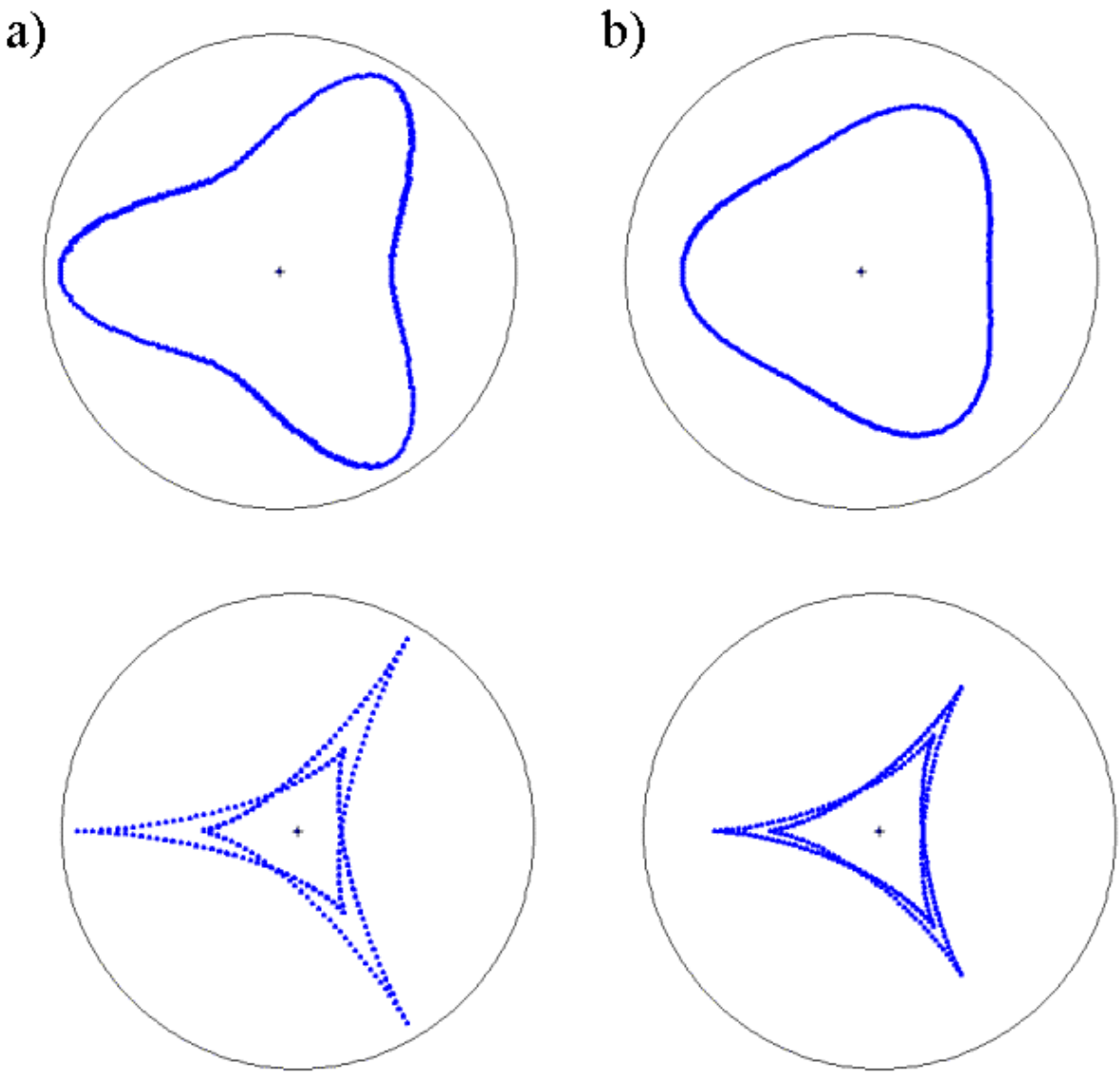

Figure 8. Parabolic lines (upper plots) and caustics (lower plots) for the *S*2 wave near the conical singularity in cubic anisotropy with varying strength. Parameters of anisotropy are: $a_{11} = 6.25$, $a_{44} = 2.08$, (a) $\gamma = 0.40$, (b) $\gamma = 0.20$. The crosses in upper plots denote the conical singularity that coincides with the vertical axis. The upper circles correspond to deviation (a) $\vartheta = 4°$, (b) $\vartheta = 2°$ of slowness directions from the vertical axis. The lower circles correspond to deviation (a) $\vartheta = 2°$, (b) $\vartheta = 0.5°$ of ray directions from the vertical axis.

Figure 9 shows two examples of anisotropy with parabolic lines crossing the conical singularity. Conditions for the occurrence of such a rather anomalous effect were studied by Shuvalov & Every (1997). The studied anisotropy has a general triclinic symmetry. The conical singularity is along the vertical axis and arose from the kiss singularity in cubic anisotropy by a small perturbation of parameters of cubic symmetry. The parameters of anisotropy are: $a_{11} = a_{22} = a_{33} = 6.25$, $a_{44} = a_{55} = a_{66} = 2.08$, $a_{12} = a_{13} = a_{23} = a_{11} - 2a_{44} + \gamma$, $a_{14} = a_{15} = a_{56} = -a_{24} = -a_{25} = -a_{46} = \varepsilon a_{11}$, with values $\varepsilon = 0.02$ and $\gamma = 3.75$ for model (a), and $\varepsilon = 0.007$ and $\gamma = 1.31$ for model (b). Anisotropy of model (b) is approximately three times lower than that of model (a). In both models, parabolic lines cross the singularity in the *S*1 (lower plots) as well as *S*2 (upper plots) slowness sheets. The figure shows that the lines even pass through the singularity and jump from one slowness sheet to the other. Figure 10 shows caustics and anticaustics generated by the conical singularity. Since the parabolic lines pass through the singularity, the caustics of the *S*1 and *S*2 waves form one closed curve. The caustics of the *S*1 and *S*2 waves are linked at six points, because six parabolic lines pass through the singularity. Moreover, the caustic touches the anticaustic at these six points. For decreasing anisotropy, parabolic lines passing through the singularity disappear and caustic around the singularity no longer touches the anticaustic.

6.3. Wedge singularity

Figure 11 shows behaviour of parabolic lines and caustics of the *S*2 wave near a wedge singularity in two anisotropic models. The models display a general triclinic symmetry, which arose by a small perturbation of cubic anisotropy. The cubic anisotropy was perturbed by adding a small but non-zero parameter a_{14}. The wedge singularity is along the vertical axis and arose by transforming the kiss singularity in cubic anisotropy. Anisotropy in model (b) is twice lower than that in model (a). In both models, parabolic lines and caustics appear in the *S*2 slowness and wave sheets only. Two pairs of parabolic lines touch the singularity. The singularity generates a linear anticaustic. The anticaustic is perpendicular to the direction of the wedge. The length of the anticaustic depends on the strength of anisotropy. With decreasing anisotropy by decreasing parameters γ and ε, the length of the anticaustic also decreases. Since parabolic lines touch the singularity, the caustic and anticaustic touch each other. If anisotropy is decreased, the parabolic lines concentrate in a closer vicinity of the singularity. For any small but non-zero parameters γ and ε, the parabolic lines always touch the singularity. For decreasing anisotropy, the shape of the parabolic line is flattening approaching a line under very weak anisotropy. Also the width of the caustic decreases more rapidly then its length. The singularity, parabolic lines, caustic and anticaustic disappear only for strictly zero parameters γ and ε.

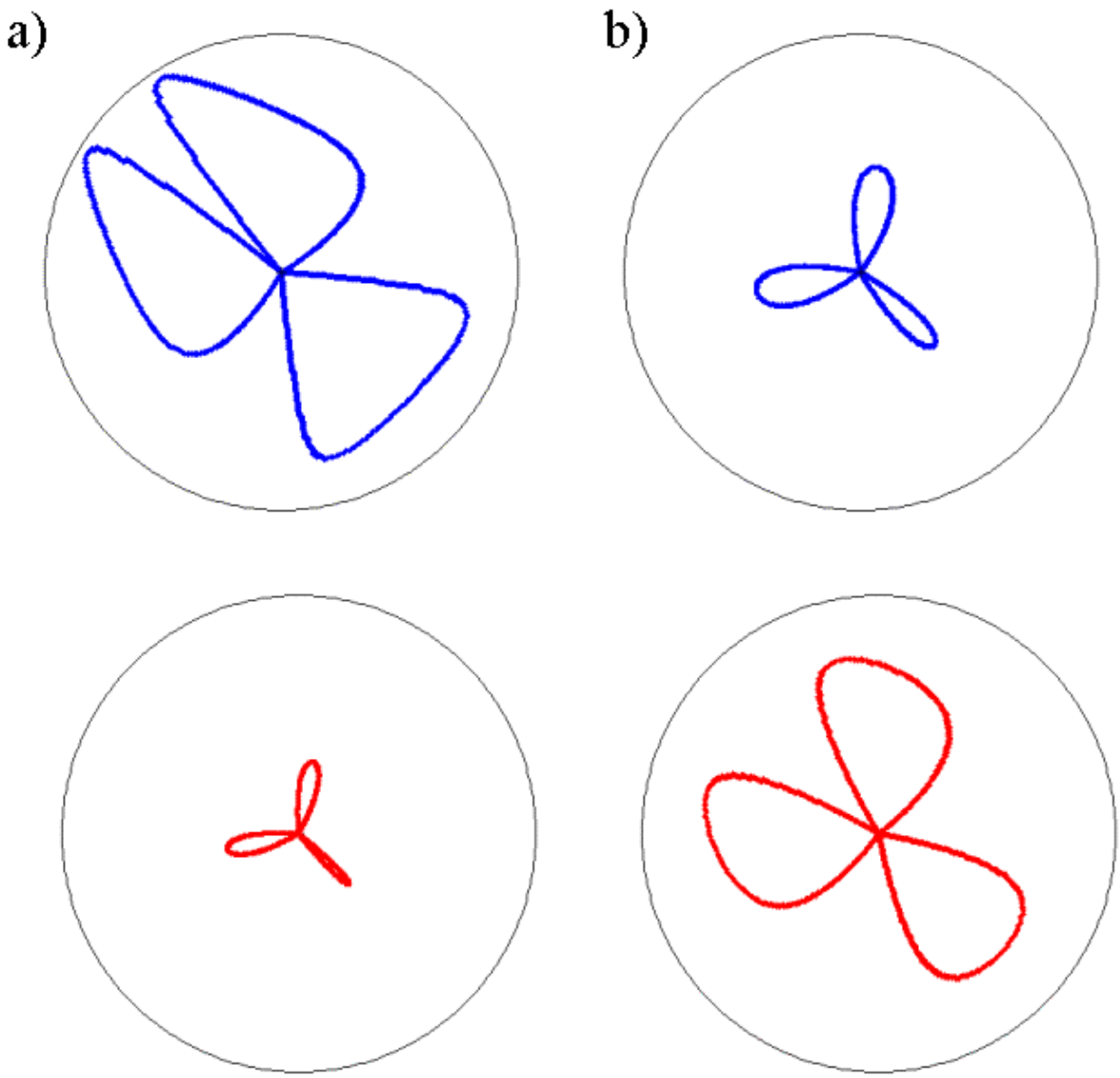

Figure 9. Parabolic lines for the $S2$ (upper plots) and $S1$ (lower plots) waves near a conical singularity for anisotropy models (a) and (b). For parameters of anisotropy, see the text. The conical singularity is along the vertical axis. The circles correspond to deviation $\vartheta = 2°$ of slowness directions from the vertical axis.

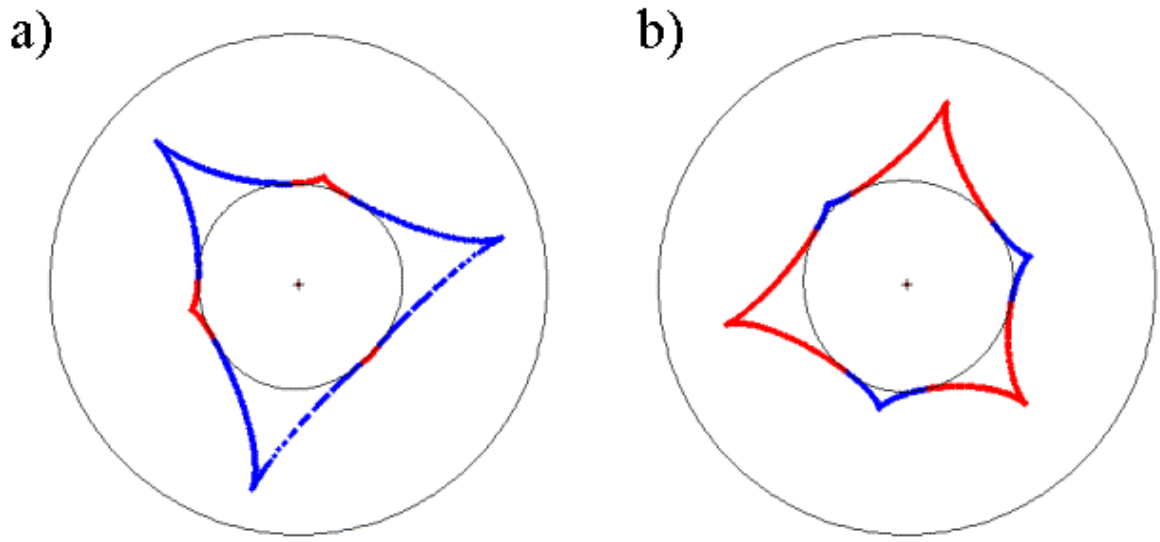

Figure 10. Caustics for the *S*1 (red) and *S*2 (blue) waves near a conical singularity for two anisotropic media. For parameters of anisotropy, see the text. The conical singularity coincides with the vertical axis. The left/right outer circle corresponds to deviation $\vartheta = 12° / 4°$ of ray directions from the vertical axis. The inner circles correspond to anticaustics generated by the conical singularity.

Conclusion

Metric tensor defined in (9) can be conveniently used for studying the shape of slowness and wave surfaces and for studying parabolic lines and caustics in anisotropic solids. No parabolic lines and caustics can appear for the *P* wave in any anisotropy including the case when the *P*-wave slowness sheet touches sheets of the other waves. Parabolic lines and caustics can appear for the *S*1 and *S*2 waves and separate convex, hyperbolic and concave areas on the slowness and wave sheets. The form of parabolic lines and caustics is, in general, more complicated for the *S*2 wave than for the *S*1 wave. The parabolic lines and caustics can appear, particularly, in the vicinity of singularities. The conical and wedge singularities also generate anticaustics. The conical singularity generates an elliptical or circular anticaustic, the wedge singularity generates a linear anticaustic. The geometry of parabolic lines and caustics can be very complicated in the vicinity of singularities. The parabolic lines can even touch a singularity: they can touch wedge and kiss singularities or pass through a conical singularity. The parabolic lines can coincide with an intersection singularity. If the parabolic lines pass through a conical singularity, then a composite caustic is generated with its branches on the *S*1 and *S*2 wave sheets. This caustic touches the anticaustic at isolated points.

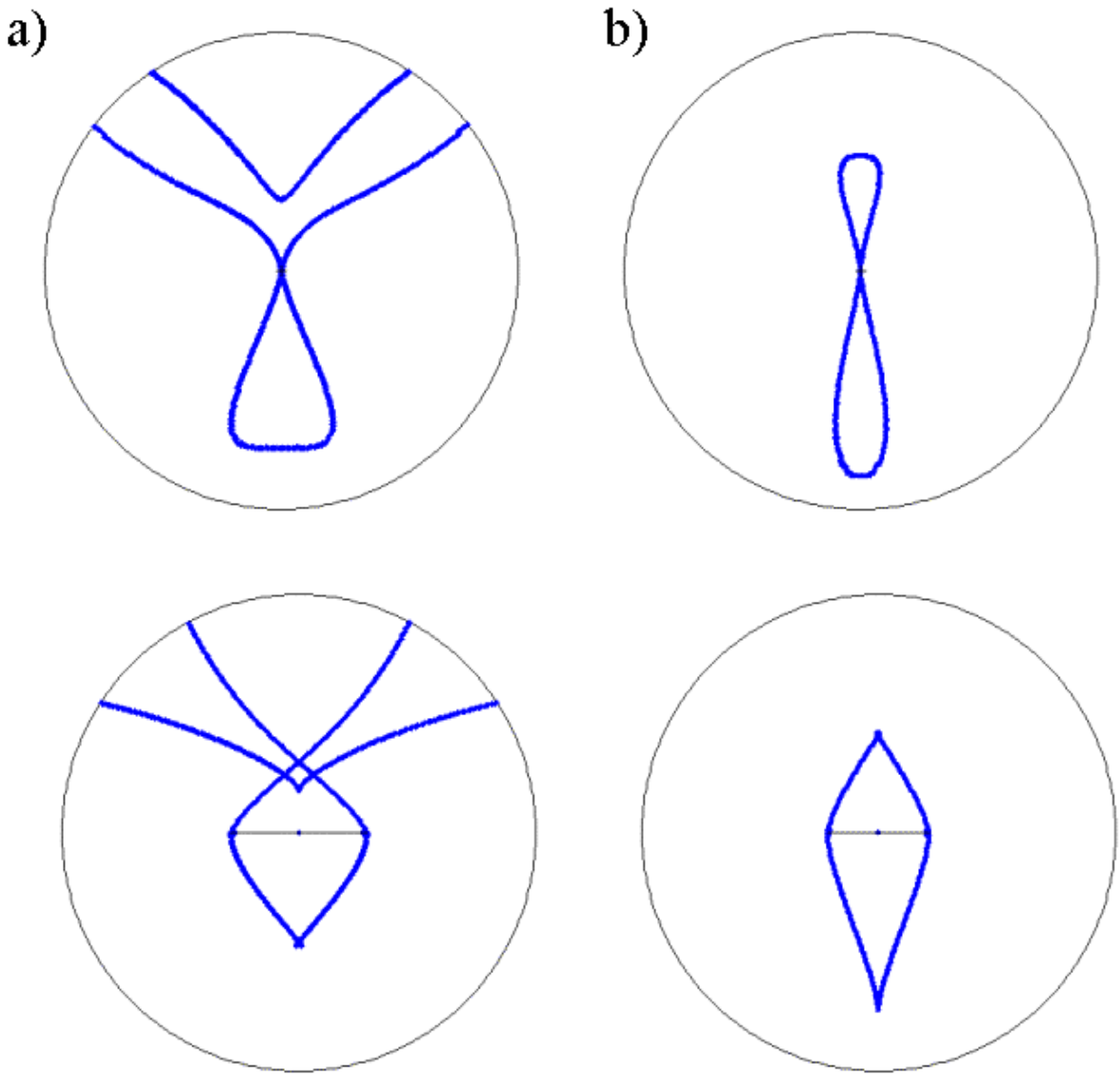

Figure 11. Parabolic lines (upper plots) and caustics (lower plots) for the *S*2 wave near a wedge singularity for anisotropy models (a) and (b). Parameters of anisotropy are: $a_{11} = 6.25$, $a_{44} = 2.08$, $a_{14} = \varepsilon a_{11}$, (a) $\gamma = 0.63$, $\varepsilon = 0.01$, (b) $\gamma = 0.31$, $\varepsilon = 0.005$. The wedge singularity is along the vertical axis. The circles in the upper plots correspond to deviation (a) $\vartheta = 5°$, (b) $\vartheta = 2.5°$ of slowness directions from the vertical axis. The circles in the lower plots correspond to deviation (a) $\vartheta = 3°$, (b) $\vartheta = 2°$ of ray directions from the vertical axis. The black line passing the vertical axis in the lower plots marks the anticaustic.

Behaviour of parabolic lines and caustics simplifies in weakly anisotropic solids. No parabolic lines and caustics appear on the *S*1 slowness and wave sheets under sufficiently weak anisotropy. Parabolic lines and caustics can appear for the *S*2 wave, but only in the directions close to conical or wedge singularities. Each conical or wedge singularity in weakly anisotropic solids generates parabolic lines, caustics and anticaustics in its vicinity. In contrary to strong anisotropy, the parabolic lines cannot pass through or touch the conical singularity in weak anisotropy. The caustic cannot touch the anticaustic. On the other hand, the parabolic lines touch each wedge singularity and caustic must touch the anticaustic near this singularity. For decreasing strength of anisotropy, the size of caustics and anticaustics decreases. For infinitesimally weak anisotropy, the caustics and anticaustics contract into one joint point. For isotropy, the conical and wedge singularities disappear together with caustics and anticaustics associated with them.

As regards transverse isotropy that is the most frequent anisotropy used, we can draw the following conclusion. Since weak transverse isotropy forms no conical or wedge singularities (Vavryčuk 1997), no parabolic lines, caustics and triplications can appear in this symmetry, provided the strength of anisotropy is sufficiently weak.

Acknowledgements

I thank V. Červený for stimulating discussions on the subject. The work was supported by the Consortium Project "Seismic waves in complex 3-D structures", and by the Grant Agency of the Czech Republic, grant No. 205/00/1350.

References

Aki, K. & Richards, P. G., 1980. *Quantitative Seismology. Theory and Methods*, W.H. Freeman, San Francisco.

Bakker, P. M., 1998. Phase shift at caustics along rays in anisotropic media, *Geophys. J. Int.*, **134**, 515-518.

Boulanger, Ph. & Hayes, M., 1998. Acoustic axes for elastic waves in crystals: theory and applications, *Proc. R. Soc. Lond.*, **A 454**, 2323-2346.

Burridge, R., 1967. The singularity on the plane lids of the wave surface of elastic media with cubic symmetry, *Q. J. Mech. Appl. Math.*, **20**, 40-56.

Červený, V., 2001. *Seismic Ray Theory*, Cambridge University Press, Cambridge.

Červený, V., 2002. Fermat's variational principle for anisotropic inhomogeneous media, *Stud. Geophys. Geod.*, **46**, in press.

Crampin, S. & Yedlin, M., 1981. Shear-wave singularities of wave propagation in anisotropic media, *J. Geophys.*, **49**, 43-46.

Every, A. G. & Kim, K. Y., 1994. Time domain dynamic response functions of elastically anisotropic solids, *J. Acoust. Soc. Am.*, **95**, 2505-2516.

Farra, V., 2001. High-order perturbations of the phase velocity and polarization of qP and qS waves in anisotropic media, *Geophys. J. Int.*, **147**, 93-104.

Grechka, V. Yu. & Obolentseva, I. R., 1993. Geometrical structure of shear wave surfaces near singularity directions in anisotropic media, *Geophys. J. Int.*, **115**, 609-616.

Helbig, K., 1994. *Foundations of Anisotropy for Exploration Seismics*, Pergamon, N.Y.

Jech, J. & Pšenčík, I., 1989. First-order perturbation method for anisotropic media, *Geophys. J. Int.*, **99**, 369-376.

Musgrave, M. J. P., 1970. *Crystal Acoustics*, Holden-Day, London.

Musgrave, M. J. P., 1985. Acoustic axes in orthorhombic media, *Proc. R. Soc. Lond.*, **A 401**, 131-143.

Payton, R.G., 1992. Wave propagation in a restricted transversely isotropic elastic solid whose slowness surface contains conical points, *Q. J. Mech. Appl. Math.*, **45**, 183-197.

Rümpker, G. & C. J. Thomson, 1994. Seismic-waveform effects of conical points in gradually varying anisotropic media, *Geophys. J. Int.*, **118**, 759-780.

Shuvalov, A.L., 1998. Topological features of the polarization fields of plane acoustic waves in anisotropic media, *Proc. R. Soc. Lond.*, **A 454**, 29112947.

Shuvalov, A.L. & Every, A.G., 1996. Curvature of acoustic slowness surface of anisotropic solids near symmetry axes, *Phys. Rev.*, **B 53**, No. 22, 14.906-14.916.

Shuvalov, A.L. & Every, A.G., 1997. Shape of the acoustic slowness surface of anisotropic solids near points of conical degeneracy, *J. Acoust. Soc. Am.*, **101**, 2381-2382.

Thomsen, L, 1986. Weak elastic anisotropy, *Geophysics*, **51**, 1954-1966.

Vavryčuk, V., 1997. Elastodynamic and elastostatic Green tensors for homogeneous weak transversely isotropic media, *Geophys. J. Int.*, **130**, 786-800.

Vavryčuk, V., 2001. Ray tracing in anisotropic media with singularities, *Geophys. J. Int.*, **145**, 265-276.

Vavryčuk, V. & Yomogida, K., 1996. *SH*-wave Green tensor for homogeneous transversely isotropic media by higher-order approximations in asymptotic ray theory, *Wave Motion*, **23**, 83-93.

Appendix A: Perturbation theory for a degenerate Christoffel eigenvalue problem

Let us assume that the Christoffel tensor Γ_{jk} is nearly degenerate

$$\Gamma_{jk} = \Gamma^0_{jk} + \Delta\Gamma_{jk} \ , \tag{A1}$$

where $\Delta\Gamma_{jk}$ is a small perturbation of degenerate tensor Γ^0_{jk} with eigenvalues

$$G^{0(1)} \neq G^{0(2)} = G^{0(3)} \equiv G^{0(23)} \ . \tag{A2}$$

The eigenvector of Γ^0_{jk} corresponding to the non-degenerate wave is $\hat{\mathbf{g}}^{0(1)}$, the eigenvectors corresponding to the degenerate waves are $\hat{\mathbf{g}}^{0(2)}$ and $\hat{\mathbf{g}}^{0(3)}$. Vectors $\hat{\mathbf{g}}^{0(2)}$ and $\hat{\mathbf{g}}^{0(3)}$ form an arbitrary orthogonal frame perpendicular to $\hat{\mathbf{g}}^{0(1)}$. Using perturbation theory (see Shuvalov 1998; Farra 2001), the eigenvalues $G^{(2)}$ and $G^{(3)}$ of Γ_{jk} can be expressed as follows

$$G^{(2),(3)} = \frac{1}{2}\left[\hat{M}^{(22)} + \hat{M}^{(33)} \pm \sqrt{\left(\hat{M}^{(22)} - \hat{M}^{(33)}\right)^2 + 4\left(\hat{M}^{(23)}\right)^2}\right] , \tag{A3}$$

$$\Delta G = G^{(2)} - G^{(3)} = \sqrt{\left(\hat{M}^{(22)} - \hat{M}^{(33)}\right)^2 + 4\left(\hat{M}^{(23)}\right)^2} \ , \tag{A4}$$

where

$$\hat{M}^{(KL)} = \hat{m}^{(KL)} + \frac{\hat{m}^{(1K)}\hat{m}^{(1L)}}{G^{0(23)} - G^{0(1)}}, \ K, L = 2,3 \ , \tag{A5}$$

$$\hat{m}^{(rs)} = \Gamma_{jk}\hat{g}^{0(r)}_j\hat{g}^{0(s)}_k, \quad r, s = 1,2,3 \ . \tag{A6}$$

If we introduce base vectors $\mathbf{g}^{0(2)}$ and $\mathbf{g}^{0(3)}$

$$\mathbf{g}^{0(2)} = \hat{\mathbf{g}}^{0(2)}\cos\Phi + \hat{\mathbf{g}}^{0(3)}\sin\Phi \ , \tag{A7}$$

$$\mathbf{g}^{0(3)} = -\hat{\mathbf{g}}^{0(2)}\sin\Phi + \hat{\mathbf{g}}^{0(3)}\cos\Phi \ , \tag{A8}$$

where angle Φ is determined from the equation

$$\tan 2\Phi = 2\frac{\hat{M}^{(23)}}{\hat{M}^{(22)} - \hat{M}^{(33)}} \ , \tag{A9}$$

we can express eigenvectors $\mathbf{g}^{(2)}$ and $\mathbf{g}^{(3)}$ as follows

$$\mathbf{g}^{(2)} = \mathbf{g}^{0(2)} + \mathbf{g}^{0(1)} \frac{m^{(12)}}{G^{0(23)} - G^{0(1)}} \ , \tag{A10}$$

$$\mathbf{g}^{(3)} = \mathbf{g}^{0(3)} + \mathbf{g}^{0(1)} \frac{m^{(13)}}{G^{0(23)} - G^{0(1)}} \ , \tag{A11}$$

Matrices $M^{(KL)}$ and $m^{(rs)}$ are calculated by (A5) and (A6) using the base vectors $\mathbf{g}^{0(r)}$, r = 1,2,3. Note that vectors $\mathbf{g}^{0(2)}$ and $\mathbf{g}^{0(3)}$ are perpendicular to $\mathbf{g}^{0(1)} = \widehat{\mathbf{g}}^{0(1)}$ similarly as vectors $\widehat{\mathbf{g}}^{0(2)}$ and $\widehat{\mathbf{g}}^{0(3)}$, hence they can serve as eigenvectors of Γ^0_{jk}. However, these eigenvectors are exceptional, because when perturbing from the degenerate tensor Γ^0_{jk} to non-degenerate tensor Γ_{jk} the transition from eigenvectors $\mathbf{g}^{0(2)}$ and $\mathbf{g}^{0(3)}$ to eigenvectors $\mathbf{g}^{(2)}$ and $\mathbf{g}^{(3)}$ is smooth. No other eigenvectors display this property. Furthermore, some formulae are simplified when using this exceptional base vectors. For example,

$$M^{(23)} = 0 \ , \tag{A12}$$

$$\Delta G = M^{(22)} - M^{(33)} \ . \tag{A13}$$

The formulae for eigenvectors/eigenvalues are valid up to the first/second order of perturbation, respectively.

Appendix B: Eigenvalues and eigenvectors of Γ_{jk} in weak anisotropy

Let us assume that the medium is weakly anisotropic

$$a_{ijkl} = a^0_{ijkl} + \Delta a_{ijkl} \ , \tag{B1}$$

$$a^0_{ijkl} = \left(\alpha^2 - 2\beta^2\right)\delta_{ij}\delta_{kl} + \beta^2\left(\delta_{ik}\delta_{jl} + \delta_{il}\delta_{jk}\right) , \tag{B2}$$

where α and β mean the *P*- and *S*-wave velocities in the isotropic reference medium, δ_{ij} is the Kronecker delta, and Δa_{ijkl} are the small perturbations of the parameters of the isotropic reference medium a^0_{ijkl}. Perturbing the Christoffel tensor we obtain

$$\Gamma^0_{jk} = \left(\alpha^2 - \beta^2\right)n_j n_k + \beta^2\delta_{jk} \ , \tag{B3}$$

$$\Delta\Gamma_{jk} = \Delta a_{ijkl} n_i n_l \ , \tag{B4}$$

where Γ_{jk}^{0} is the Christoffel tensor in the isotropic reference medium, and $\Delta\Gamma_{jk}$ is its perturbation. If we introduce weak anisotropy tensor b_{ijkl}

$$\Delta a_{ijkl} = \varepsilon\, b_{ijkl}\,, \tag{B5}$$

where ε is a small parameter, we can express ΔG as follows

$$\Delta G = G^{(2)} - G^{(3)} = \varepsilon\sqrt{\left(\widehat{\mathbf{u}}^{b(23)}\cdot\mathbf{n} + \varepsilon\,\mathbf{n}^T\widehat{\mathbf{F}}\mathbf{n}\right)^2 + \left(\widehat{\mathbf{v}}^{b(23)}\cdot\mathbf{n} + \varepsilon\,\mathbf{n}^T\widehat{\mathbf{G}}\mathbf{n}\right)^2}\,, \tag{B6}$$

where

$$\widehat{u}_i^{b(rs)} = b_{ijkl}n_l\left(\widehat{g}_j^{0(r)}\widehat{g}_k^{0(r)} - \widehat{g}_j^{0(s)}\widehat{g}_k^{0(s)}\right)\,,\quad \widehat{v}_i^{b(rs)} = b_{ijkl}n_l\left(\widehat{g}_j^{0(r)}\widehat{g}_k^{0(s)} + \widehat{g}_j^{0(s)}\widehat{g}_k^{0(r)}\right)\,, \tag{B7}$$

$$\widehat{F}_{il} = \frac{1}{4}\frac{\widehat{v}_i^{b(12)}\widehat{v}_l^{b(12)} - \widehat{v}_i^{b(13)}\widehat{v}_l^{b(13)}}{\beta^2-\alpha^2}\,,\quad \widehat{G}_{il} = \frac{1}{2}\frac{\widehat{v}_i^{b(12)}\widehat{v}_l^{b(13)} + \widehat{v}_i^{b(13)}\widehat{v}_l^{b(12)}}{\beta^2-\alpha^2}\,. \tag{B8}$$

Vectors $\mathbf{g}^{0(2)}$ and $\mathbf{g}^{0(3)}$ are defined in (A7) and (A8) with angle Φ

$$\tan 2\Phi = \frac{\widehat{\mathbf{v}}^{b(23)}\cdot\mathbf{n} + \varepsilon\,\mathbf{n}^T\widehat{\mathbf{G}}\mathbf{n}}{\widehat{\mathbf{u}}^{b(23)}\cdot\mathbf{n} + \varepsilon\,\mathbf{n}^T\widehat{\mathbf{F}}\mathbf{n}}\,. \tag{B9}$$

For eigenvectors $\mathbf{g}^{(2)}$ and $\mathbf{g}^{(3)}$ we obtain

$$\mathbf{g}^{(2)} = \mathbf{g}^{0(2)} + \frac{1}{2}\varepsilon\,\mathbf{g}^{0(1)}\frac{\mathbf{v}^{b(12)}\cdot\mathbf{n}}{\beta^2-\alpha^2}\,, \tag{B10}$$

$$\mathbf{g}^{(3)} = \mathbf{g}^{0(3)} + \frac{1}{2}\varepsilon\,\mathbf{g}^{0(1)}\frac{\mathbf{v}^{b(13)}\cdot\mathbf{n}}{\beta^2-\alpha^2}\,, \tag{B11}$$

where $\mathbf{g}^{0(1)}$ equals **n**, and vectors $\mathbf{v}^{b(12)}$ and $\mathbf{v}^{b(13)}$ are calculated by (B7) using the base vectors $\mathbf{g}^{0(r)}$, r = 1,2,3.

The formulae for eigenvectors/eigenvalues are valid up to the first/second order of perturbation, respectively.

Appendix C: Eigenvalues and eigenvectors of Γ_{jk} in the vicinity of a singularity

All quantities in the singularity will be denoted by superscript 0. The slowness direction is perturbed as follows

$$\mathbf{n} = \mathbf{n}^0 + \Delta\mathbf{n}\,,\ \Delta\mathbf{n} = \vartheta\,\mathbf{e} - \frac{1}{2}\vartheta^2\mathbf{n}^0, \tag{C1}$$

where $\mathbf{e}$ is an arbitrary unit vector orthogonal to $\mathbf{n}^0$, and ϑ is the angle between $\mathbf{n}$ and $\mathbf{n}^0$ that must be small. Perturbing the Christoffel tensor we obtain

$$\Gamma_{jk}^0 = a_{ijkl} n_i^0 n_l^0\ , \tag{C2}$$

$$\Delta\Gamma_{jk} = a_{ijkl}\left(\Delta n_i n_l^0 + \Delta n_l n_i^0\right) + a_{ijkl}\Delta n_i \Delta n_l\ . \tag{C3}$$

Inserting (C2) and (C3) into (A4) we get (see Shuvalov 1998, Eqs 2.11-2.17)

$$\Delta G = \vartheta\ \sqrt{\left(2\hat{\mathbf{u}}^{0(23)}\cdot\mathbf{e} + \vartheta\,\mathbf{e}^T\hat{\mathbf{F}}\mathbf{e}\right)^2 + \left(2\hat{\mathbf{v}}^{0(23)}\cdot\mathbf{e} + \vartheta\,\mathbf{e}^T\hat{\mathbf{G}}\mathbf{e}\right)^2}\ , \tag{C4}$$

where

$$\hat{u}_i^{0(rs)} = a_{ijkl} n_l^0 \left(\hat{g}_j^{0(r)}\hat{g}_k^{0(r)} - \hat{g}_j^{0(s)}\hat{g}_k^{0(s)}\right),\ \ \hat{v}_i^{0(rs)} = a_{ijkl} n_l^0 \left(\hat{g}_j^{0(r)}\hat{g}_k^{0(s)} + \hat{g}_j^{0(s)}\hat{g}_k^{0(r)}\right), \tag{C5}$$

$$\hat{F}_{il} = a_{ijkl}\left(\hat{g}_j^{0(2)}\hat{g}_k^{0(2)} - \hat{g}_j^{0(3)}\hat{g}_k^{0(3)}\right) + \frac{\hat{v}_i^{0(12)}\hat{v}_l^{0(12)} - \hat{v}_i^{0(13)}\hat{v}_l^{0(13)}}{G^{0(23)} - G^{0(1)}}\ , \tag{C6}$$

$$\hat{G}_{il} = a_{ijkl}\left(\hat{g}_j^{0(2)}\hat{g}_k^{0(3)} + \hat{g}_j^{0(3)}\hat{g}_k^{0(2)}\right) + \frac{\hat{v}_i^{0(12)}\hat{v}_l^{0(13)} + \hat{v}_i^{0(13)}\hat{v}_l^{0(12)}}{G^{0(23)} - G^{0(1)}}\ . \tag{C7}$$

Vectors $\mathbf{g}^{0(2)}$ and $\mathbf{g}^{0(3)}$ are defined in (A7) and (A8) with angle Φ

$$\tan 2\Phi = \frac{2\hat{\mathbf{v}}^{0(23)}\cdot\mathbf{e} + \vartheta\,\mathbf{e}^T\hat{\mathbf{G}}\mathbf{e}}{2\hat{\mathbf{u}}^{0(23)}\cdot\mathbf{e} + \vartheta\,\mathbf{e}^T\hat{\mathbf{F}}\mathbf{e}}\ . \tag{C8}$$

For eigenvectors $\mathbf{g}^{(2)}$ and $\mathbf{g}^{(3)}$ we obtain

$$\mathbf{g}^{(2)} = \mathbf{g}^{0(2)} + \vartheta\,\mathbf{g}^{0(1)}\frac{\mathbf{v}^{0(12)}\cdot\mathbf{e}}{G^{0(23)} - G^{0(1)}}\ . \tag{C9}$$

$$\mathbf{g}^{(3)} = \mathbf{g}^{0(3)} + \vartheta\,\mathbf{g}^{0(1)}\frac{\mathbf{v}^{0(13)}\cdot\mathbf{e}}{G^{0(23)} - G^{0(1)}}\ , \tag{C10}$$

where vectors $\mathbf{v}^{0(12)}$ and $\mathbf{v}^{0(13)}$ are calculated by (C5) using the base vectors $\mathbf{g}^{0(r)}$, r = 1,2,3.

The formulae for eigenvectors/eigenvalues are valid up to the first/second order of perturbation, respectively.

Appendix D: Metric tensor in weakly anisotropic solids

Linearizing the *S*1-wave metric tensor $H_{il}^{(2)}$ in (17) for weakly anisotropic solids, we obtain

$$H_{il}^{(2)} = H_{il}^{0(2)} + \Delta H_{il}^{(2)}, \tag{D1}$$

$$H_{il}^{0(2)} = \left[a_{ijkl} g_j^{(2)} g_k^{(2)}\right]^0 + \left[\frac{v_i^{(12)} v_l^{(12)}}{G^{(2)} - G^{(1)}}\right]^0 + \left[\frac{v_i^{(23)} v_l^{(23)}}{G^{(2)} - G^{(3)}}\right]^0 , \tag{D2}$$

$$\Delta H_{il}^{(2)} = \Delta\left[a_{ijkl} g_j^{(2)} g_k^{(2)}\right] + \Delta\left[\frac{v_i^{(12)} v_l^{(12)}}{G^{(2)} - G^{(1)}}\right] + \Delta\left[\frac{v_i^{(23)} v_l^{(23)}}{G^{(2)} - G^{(3)}}\right] , \tag{D3}$$

where $H_{il}^{0(2)}$ is the leading term of the metric tensor, and $\Delta H_{il}^{(2)}$ is its perturbation.

The leading term $H_{il}^{0(2)}$ can further be simplified using the following identities

$$\left[a_{ijkl} g_j^{(2)} g_k^{(2)}\right]^0 = a_{ijkl}^0 g_j^{0(2)} g_k^{0(2)} = \left(\alpha^2 - \beta^2\right) g_i^{0(2)} g_l^{0(2)} + \beta^2 \delta_{il} , \tag{D4}$$

$$\left[\frac{v_i^{(12)} v_l^{(12)}}{G^{(2)} - G^{(1)}}\right]^0 = \frac{v_i^{0(12)} v_l^{0(12)}}{G^{0(2)} - G^{0(1)}} = -\left(\alpha^2 - \beta^2\right) g_i^{0(2)} g_l^{0(2)} , \tag{D5}$$

$$\left[\frac{v_i^{(23)} v_l^{(23)}}{G^{(2)} - G^{(3)}}\right]^0 = \frac{v_i^{0(23)} v_l^{0(23)} + \Delta v_i^{(23)} v_l^{0(23)} + v_i^{0(23)} \Delta v_l^{(23)}}{\Delta G} = 0 , \tag{D6}$$

where we used

$$a_{ijkl}^0 = \left(\alpha^2 - 2\beta^2\right) \delta_{ij} \delta_{kl} + \beta^2 \left(\delta_{ik} \delta_{jl} + \delta_{il} \delta_{jk}\right) , \tag{D7}$$

$$G^{0(1)} = \alpha^2 , \; G^{0(2)} = G^{0(3)} = \beta^2 , \tag{D8}$$

$$v_i^{0(12)} = a_{ijkl}^0 n_l \left(g_j^{0(1)} g_k^{0(2)} + g_j^{0(2)} g_k^{0(1)}\right) = \left(\alpha^2 - \beta^2\right) g_i^{0(2)} , \tag{D9}$$

$$v_i^{0(23)} = a_{ijkl}^0 n_l \left(g_j^{0(2)} g_k^{0(3)} + g_j^{0(3)} g_k^{0(2)}\right) = 0 . \tag{D10}$$

Quantity $\Delta G = G^{(2)} - G^{(3)}$ is small and positive. Using (D4)-(D6) we obtain for the leading term $H_{il}^{0(2)}$

$$H_{il}^{0(2)} = \beta^2 \delta_{il} . \tag{D11}$$

The first-order perturbation terms in (D3) are expressed as

$$\Delta\left[a_{ijkl}g_j^{(2)}g_k^{(2)}\right]=\Delta a_{ijkl}g_j^{0(2)}g_k^{0(2)}+a_{ijkl}^0\left(\Delta g_j^{(2)}g_k^{0(2)}+g_j^{0(2)}\Delta g_k^{(2)}\right)\,, \tag{D12}$$

$$\Delta\left[\frac{v_i^{(12)}\,v_l^{(12)}}{G^{(2)}-G^{(1)}}\right]=\frac{\Delta v_i^{(12)}\,v_l^{0(12)}+v_i^{0(12)}\,\Delta v_l^{(12)}}{G^{0(2)}-G^{0(1)}}-v_i^{0(12)}\,v_l^{0(12)}\frac{\Delta G^{(2)}-\Delta G^{(1)}}{\left(G^{0(2)}-G^{0(1)}\right)^2}\,, \tag{D13}$$

$$\Delta\left[\frac{v_i^{(23)}\,v_l^{(23)}}{\Delta G}\right]=\frac{\Delta v_i^{(23)}\,\Delta v_l^{(23)}}{\Delta G}\,, \tag{D14}$$

where ΔG is defined in (B6). Inserting (D7)-(D9) into (D12)-(D14), we obtain for $\Delta H_{il}^{(2)}$

$$\begin{aligned}\Delta H_{il}^{(2)} &= \Delta a_{ijkl}g_j^{0(2)}g_k^{0(2)}+\left(\alpha^2-\beta^2\right)\left(\Delta g_i^{(2)}g_l^{0(2)}+g_i^{0(2)}\Delta g_l^{(2)}\right)-g_i^{0(2)}\Delta v_l^{(12)}-g_l^{0(2)}\Delta v_i^{(12)}\\ &\quad -g_i^{0(2)}g_l^{0(2)}\left(\Delta G^{(2)}-\Delta G^{(1)}\right)+\frac{\Delta v_i^{(23)}\Delta v_l^{(23)}}{\Delta G}\,.\end{aligned} \tag{D15}$$

Analogously, we obtain the formula for the metric tensor of the *S*2 wave:

$$H_{il}^{0(3)}=\beta^2\delta_{il}\,, \tag{D16}$$

$$\begin{aligned}\Delta H_{il}^{(3)} &= \Delta a_{ijkl}g_j^{0(3)}g_k^{0(3)}+\left(\alpha^2-\beta^2\right)\left(\Delta g_i^{(3)}g_l^{0(3)}+g_i^{0(3)}\Delta g_l^{(3)}\right)-g_i^{0(3)}\Delta v_l^{(13)}-g_l^{0(3)}\Delta v_i^{(13)}\\ &\quad -g_i^{0(3)}g_l^{0(3)}\left(\Delta G^{(3)}-\Delta G^{(1)}\right)-\frac{\Delta v_i^{(23)}\Delta v_l^{(23)}}{\Delta G}\,.\end{aligned} \tag{D17}$$